NAZARBAYEV UNIVERSITY

EME-451 CAPSTONE I

Numerical and Experimental Investigation of multiphase flows. Fundamental and Applied studies

Student name and ID: Asset Zhamiyev
Nurzhan Maldenov
Bekbolat Adekenov
Arman Abylkassimov

Supervisor: Sholpan Sumbekova
Michael Yong Zhao

Date of Submission: 24.11.2019

Abstract

Multiphase flows can be met both in nature and in industrial processes. The particular case of multiphase flows is particle-laden flows, consisting of fluid phase and particle phase. Study is aimed at the investigation of the dynamics of particles in laminar and turbulent flows. The dynamics of particles depends on their physical properties. The study of the particle's dynamics in turbulent flow consisted of three parts: simulation of homogeneous isotropic turbulence (HIT), simulation of particle-laden flows and investigation of particles' pair dispersion. Initially, the turbulent flow was simulated in OpenFOAM via Large Eddy simulation (LES) and Direct Navier Stokes (DNS) methods. Then not decaying homogeneous isotropic turbulence was achieved by addition of forcing term. The effect of different values of forcing constant on turbulent flow was investigated. The mesh convergence study was performed for LES and DNS. Results showed convergence in LES simulations and the reduction of volume-averaged velocity fluctuations (U') in DNS with an increase of the number of mesh elements. The particle phase simulation was performed in Matlab and CFDEM. The simulation in Matlab revealed several constraints. The simulation of particles with turbulence phase for a short period of time was performed in CFDEM. However, due to the decaying nature of the flow, the investigation of particles' trajectories could not be performed. The pair dispersion of inertial particles in turbulent flow was investigated for available experimental data. The results were represented on graphs with normalized scales. The correlation between the velocity of flow and the normalized value of the initial separation was determined. The mean square separation does not change significantly until the first decade. The motion of clots in blood flow was numerically simulated using Ansys Fluent package. The mesh convergence study was performed and the velocity of the particles in blood flow was analyzed. The results obtained for blood flow showed distribution close to Gaussian. The preliminary experiment was conducted for small particles of smoke. The smoke cloud was detected via the image intensity analysis.

Table of Contents

1. Introduction

Multiphase flows are widespread and can be found both in natural phenomena such as the formation of clouds and sedimentation in rivers [1] and numerous industrial processes including coal combustion, pipeline pneumatic transport [2, 3]. Therefore, the study of the nature of these processes is important both for fundamental science and for industry. The particular case of multiphase flows is particle-laden flows. Particle-laden flows consist of fluid and particles phases, typically liquid droplets or solid particles. The particle-laden flows can be laminar and turbulent. The dynamics of particles in a turbulent flow is affected by the flow; however, the degree of influence of the flow on the motion of particles depends on the physical properties of the particles. The main mechanisms influencing the behavior of particles in the flow are viscous drag exerted from turbulence to particles and gravitational force. If the density of particles is approximately the same as of fluid (neutrally buoyant particles) and the size of particles is small (much less than the smallest turbulent eddies at the Kolmogorov scale), particles behave as tracers following the motion of the flow [4]. Kolmogorov scale is the smallest scale of turbulence, which is characterized by domination of viscous forces over fluid inertia [5]. The acceleration and vorticity of the turbulence in Kolmogorov scale is maximum. Being less than Kolmogorov scale tracers are exposed mostly to the drag force [6]. However, if the density of particles is considerably smaller or larger than the density of fluid, or when the size of particles becomes of the same order as the turbulent eddies, the motion of particles is affected by the inertial effects and gravitational force. Such particles are called inertial particles and their motion deviates from the flow. The inertial effects of particles is quantified by calculation of Stokes number (St).

$$St = \frac{\tau_p}{\tau_\eta}, \qquad (1)$$

Where τ_p – particle response time, τ_η – Kolmogorov time scale

Inertial particles lag behind the flow, and particle response time is time required to particle to respond to the change of the flow's velocity. Kolmogorov time scale – time of energy dissipation at Kolmogorov scale [5]. Being in a turbulent flow, inertial particles are centrifuged due to the interaction with turbulent vortices and cluster in the zones of high strain and low vorticity [6]. Finally, as the time passes the particle settle under the influence of gravitation. The study conducted by Wang and Maxey [7] demonstrated that the preferential sweeping is the prevailing mechanism in a turbulent flow. The inertial particles distribute unevenly in a turbulent non-uniform flow, clustering in the regions of high strain rate and low vorticity. The mechanism of accumulation of particles in certain regions is called the preferential concentration [8]. Maxey demonstrated that the preferential concentration results in a bias of particles' motion and enhanced settling velocity.

The reduction of particle settling velocity is related to three mechanisms: nonlinear drag, vortex trapping and loitering effect [9]. The different studies conducting on the effect of nonlinear drag on the reduction of particles' settling rate provide controversial data. The results obtained by Mei [10] and Stout et al. [11] demonstrated the reduction of settling velocity related to nonlinear drag. The results obtained by Stout et al. show that the reduction of average settling velocity may exceed 35%. At the same time, the analytical solution derived by Nielsen [12] indicated the negligible effect of drag ($>10^{-5}$VT). Vortices in a turbulent flow tend to trap inertial particles temporally (forming vortex trap) and transport them over certain distances, finally flinging particles [13]. Being trapped in vortices particles are affected by the motion of vortices and, therefore, their settling rate is reduced. The numerical results of Vilela and Motter [14] demonstrated the possibility of the vortex traps in the presence of large gravitational force for

aerosol particles in leepfrog system and blinking vortex system. The loitering effect was firstly observed by Nielsen [12]. Loitering is the effect describing the reduction of particle settling rate happening when fast-moving particles pass through regions of flow moving upward and downward. The particle requires more time to cross the upward-moving regions. The observations of Nielsen were further confirmed by Good et al. [15].

The particles-laden laminar flows characterized by low velocity as well as high viscosity could be found in engineering applications involving flows in circular ducts, natural convection and air ventilating processes. The-two phase flows in coronary arteries, in which the carrier fluid is non-Newtonian blood and the particle phase represented by fragmented blood clots proceed under laminar regime. That is due to the high blood viscosity and relatively low values of inner artery diameters and average outlet velocities. The curved circular blood vessels that supply oxygen-rich blood to the myocardium are defined as coronary arteries. The Reynolds number based on inlet and outlet velocities are found to be less than 2300 implying laminar flow field [16]. The stable and continuous blood supply ought to be delivered to the heart to sustain its optimal cardiac functions and cycle. Atherosclerosis, which is the form of cardiovascular disease, contributes to the formation of plaque on the vessel wall. As a results, the coronary artery narrows, thereby restricting the blood supply to myocardium. Stenosis is related to the increased plaque accumulation and results to the narrowing of aortic valve area, leading to the rapid advancement of the coronary artery disease [17]. The alteration of blood flow due to narrowing artery facilitate clots formation. The fragmented clots lag behind the blood flow due to higher density and behave as inertial particles with complex flow structures dispersed in blood stream [18]. The clot formation leads to an advancement of unwanted diseases like stroke, paralysis, heart attack that require immediate medical treatment. According to World Health Organization data (2019), the cardiovascular disease (CVD) is the major cause of people mortality all over the globe. Around 80% of all deaths worldwide associated with CVDs occur in countries with low and middle income [19]. The investigation of dynamics of inertial particles in laminar flow may be used for determination of the location of stenosis in arteries. Thereby, the amount of deaths due to CVDs can be reduced.

This paper is aimed at in-depth investigation of the multiphase flows on the examples of laminar and turbulent particle-laden flows. The study consists of the numerical simulations of inertial particles in turbulent flow and applied biomechanics study – the investigation of the particles in arteries. Additionally, the study contains experimental part. The simulations of the particle-laden turbulent flow are performed via direct Navier-Stokes (DNS) and large eddy simulations (LES) methods in OpenFOAM software. The simulations of particle phase are performed in Matlab and CFDEM. The simulation of the multiphase flow in arteries are performed in ANSYS Fluent package.

2. Background information

2.1 Homogeneous Isotropic Turbulence

Homogeneous isotropic turbulence (HIT) is one of the forms of idealistic turbulence flow that can be modeled with numerical simulation. Statistical parameters are invariant of coordinate system of domain of study in HIT. DNS and LES are commonly applied to HIT flows and generated turbulence field is used in particle tracking simulations **[19][20][21].** HIT is not statistically stationary and velocity fluctuations tend to decrease to zero with time evolution until it reaches zero. Statistically stationary field is achieved when the field averaged dissipation rate is equal to energy addition rate. **[21]** Stochastic forcing mechanism is developed based on the assumption that small scales are not affected by the mechanisms of forcing scheme if there is the same level of energy-production and dissipation in a turbulent flow. Based on this method, velocity field is transformed into Fourier space as shown in equation below,

$$\underline{\tilde{u}}(\underline{k},t) = \sum_N \sum_N \sum_N \underline{u}(\underline{x},t) e^{-i\underline{k}\cdot\underline{x}}, \quad (2)$$

Where $\underline{u}(\underline{x},t)$ – velocity at grid point inflow domain, $\underline{\tilde{u}}(\underline{x},t)$ – corresponding Fourier coefficient to this point. Forcing is added to acceleration equation as shown in (3)

$$\frac{\partial \underline{\tilde{u}}(\underline{x},t)}{\partial t} = \underline{\tilde{a}}(\underline{k},t) + \underline{\tilde{a}}^F(\underline{k},t) \quad (3)$$

Where $\underline{\tilde{a}}^F(\underline{k},t)$ is forcing term that is non-zero for$k \in [0, K_F]$. Forcing acceleration term is modelled with Uhlenbeck-Ornstein (UO) random process **[22]** where main controllable variables are acceleration variance σ and forcing time constant (α).

$$\alpha = \frac{1}{t_f} \quad (4)$$

Where t_f – time period in which the forcing term is added to the flow (forcing time)

The relation between the forcing time scale and HIT flow field properties were studied when stochastic forcing was implied to add kinetic energy at large scales. Results of DNS revealed that flow dissipation rate and flow Reynolds number are affected by forcing time scale, t_f. It was found that increased t_f, values results in an increase of vortical structure size **[20]**. Energy dissipation rate did not change for values of t_f.smaller than 10% of eddy turnover time (T_e) [9]. This was also true for Taylor microscale flow Reynolds number and integral length scale.

Radial Distribution Function (RDF) is used to quantify the impact of preferential concentration of droplet on the collision rate. Series of simulations show that RDF value is not sensitive to t_f, if forcing time scale is set less than Kolmogorov time scale ($t_f < t_\eta$]). It is recommended to use t_f value in range of [$dt\ t_\eta$] where dt is time step. It will eliminate undesirable impact of t_f parameter on HIT flow characteristics and particle clustering process.

Another important turbulence characteristics is the energy spectrum of turbulence field scales. Normalized energy spectrum of turbulence field for different t_f.can be seen in **Figure 1.** Energy spectrum can be thought of kinetic energy stored in each scale of velocity field, since **Equation (2)** has transformed velocity field into Fourier space.

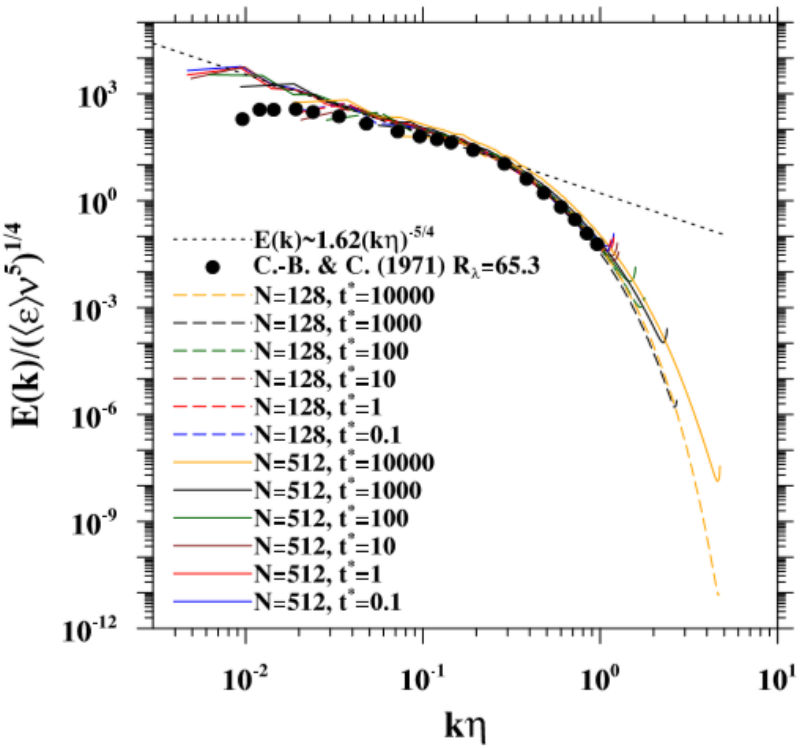

Figure 1 Energy Spectrum of turbulence field for different N at various values of t_f [20]

The effect of different large scale forcing schemes on quantitative collision statistics of particle simulation has been investigated with DNS simulations. Level of particle clustering in the flow can directly be affected by the value of RDF. RDF value of 6.584 cm^3/s and 6.301 cm^3/s was obtained for particle size of 20μm by stochastic and deterministic methods. This kind of noticeable difference between two large scale forcing schemes was also observed by **[23], [24]** Results of dynamic and kinematic collision kernels show negligible difference between two forcing methods with deterministic forcing scheme showing larger collision kernel values for droplet size of larger than 30μm.

Based on the findings of **[25], [26],** it is possible to state that stochastic forcing can be applied alone to generate HIT field and achieve statistically almost the same HIT. Simulation of HIT with cloud droplets is computationally expensive. Parallel computing algorithms are required to speed up the solution by keeping the flow characteristics. Scalability of parallel computing was studied with mesh resolution of 512^2 and 1024^2 and 10^6-10^7 droplets. This study has found a linear relation between execution time of simulation and number of processors being used for calculation. [27 The simulation code for parallel computing was first implemented in previous works by **[28].** This solver quantitatively evaluates the effects of turbulent flow and hydrodynamic interactions of fluid and small particles with hybrid DNS solver. The parallel computing approach is going to be implemented in this study to increase the computational time efficiency.

2.2 Dynamics of particle phase

Depending in the flow-particle interaction there are several coupling models. In reality, the inertial particles are affected by the turbulence, while the flow is influenced by the particles. Additionally, the motion of particles changes due to the collisions of particles. However, for highly dilute flows, the influence of particles is small and can be neglected. The collisions of particles have

insignificant effect on their motion. According to Elghobashi [29], the effect of particles can be ignored if the volume fraction of the particles (α_p) is less than or equal to 10^{-6}.

$$\alpha_p = \frac{V_p}{V}, (5)$$

Where V_p – volume of particles, V – volume of turbulent flow.
The classification of particle-laden turbulent flows is presented in the figure below.

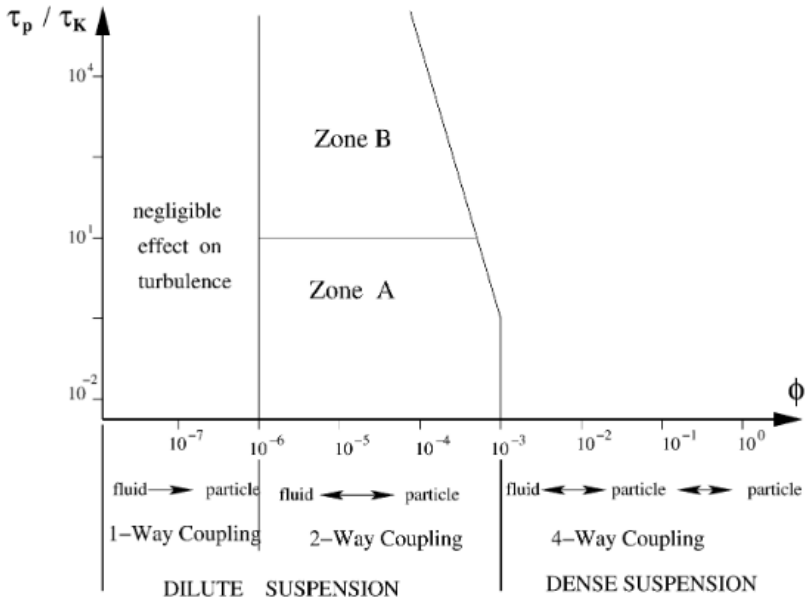

Figure 2. Classification of particle-laden turbulent flows based on volume fraction [29]

Therefore, the for highly diluted flows, the only interaction between the particles is approximated to particle-flow interaction with no influence of particles on the flow. Such coupling method is called one-way coupling. The good convergence of one-way coupled simulations with experimental data at low values of volume fraction is supported by the results of numerous studies [30]. Two-way coupled simulations consider also the effect of particles on the flow, whereas four-way coupled simulations include particle-particle interaction in addition to the above [31].

The dynamics of inertial particles is governed by two main parameters – St (Stokes number) and Sv (Settling rate). Stokes number quantifies the inertia of a particle, whereas the settling rate compares the velocity of a particle in a still fluid with flow Kolmogorov velocity [32].

$$St = \frac{\tau_p}{\tau_k} = \frac{2\rho_p \varepsilon^{0.5} a^2}{9\rho_f \nu^{1.5}} \quad (6)$$

$$S_v = \frac{V_T}{\nu_k} = \frac{2\rho_p g a^2}{9\rho_f \varepsilon^{0.25} \nu^{1.25}}, \quad (7)$$

Where τ_p – particle response time, τ_k – Kolmogorov time, ρ_p – density of particles, ρ_f – density of fluid, ε – energy dissipation rate, ν – fluid kinematic viscosity, a – particle's radius, V_T – particle's terminal velocity in still fluid, ν_k – flow Kolmogorov velocity, g – gravitational acceleration.

From equations (6) and (7) it can be seen that the dynamics of the inertial particles in turbulent flow depends on five physical parameters. The motion of inertial particles in turbulent flow is described by the Maxey-Riley equations [16].

$$\frac{dV^{(k)}(t)}{dt} = -f(Re, V_{rel})\frac{V^{(k)}(t) - U(Y^{(k)}(t), t)}{\tau_p^{(k)}} + g \quad (8)$$

$$\frac{dY^{(k)}(t)}{dt} = V^{(k)}(t), \quad (9)$$

Where V – velocity of the particle, t – time, U – velocity of the field, Y – position of the particle, f – drag coefficient (set to 1), k – particle's subscript.

2.3 Murray's Law

Murray's Law is implemented to estimate the blood flow at the outlets of vascular system. As stated by this law, the cubic diameter of vascular system's parent vessel is equal to the sum of cubes of its daughter vessels. Figure 1 illustrates the bifurcation geometry of the blood vessel for which equation $D_0^3 = D_1^3 + D_2^3$ is valid. In addition, the volume flow rate of the vessel branch is proportional to its cubic diameter [33].

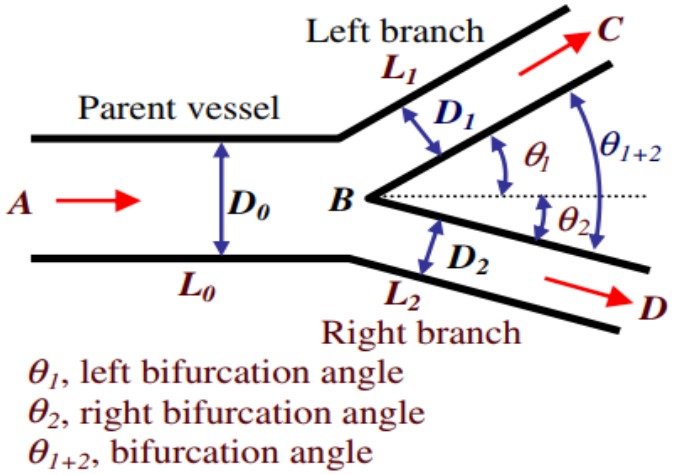

Figure 3. Geometry of bifurcation vessel

The human coronary artery represents the branched tree with one inlet and multiple outlet vessels. The three-dimensional model of artery could be obtained from the segmentation of Computer Tomography images. The modified equation representing Murray's Law could be written as follows:

$$Q = \sum_{i=1}^{n} Q_j = \sum_{i=1}^{n} \alpha_j Q = \sum_{i=1}^{n} \frac{d_j^3}{d_1^3 + d_2^3 + \ldots + d_n^3} Q, \quad (10)$$

where n-number of outlet branches, Q_j- flow rate at j-th outlet, d-vessel diameter,

$\alpha_j = \frac{d_j^3}{d_1^3 + d_2^3 + \ldots + d_n^3}$ is coefficient of proportionality.

The above equation enables to estimate the flow rate at each outlet assuming the branch sizes and total flow rate are known. The diameter values are calculated from the surface area of corresponding boundaries.

Table 1. Outlet flow rates (calculated by Murray's law and Re numbers for CHN03 artery model)

#	Surface Area, mm^2	D,mm	D^3, mm^3	Alpha	Qi, cm^3/s	mass flow, kg/s	V, m/s	Re
Inlet	9.06	3.40						613.99
Outlet 1	2.57	1.81	5.91	0.22	1.38	0.00147	0.54	258.40
Outlet 2	2.23	1.68	4.77	0.18	1.12	0.00119	0.50	224.05
Outlet 3	2.19	1.67	4.67	0.18	1.09	0.00116	0.50	220.71
Outlet 4	1.82	1.52	3.53	0.13	0.83	0.00088	0.45	183.24
Outlet 5	1.78	1.50	3.41	0.13	0.80	0.00085	0.45	178.98
Outlet 6	2.01	1.60	4.10	0.16	0.96	0.00102	0.48	202.54
Sum			26.39		6.18			
Qtot, cm^3/s	6.18							
V_inlet, m/s	0.68							

Table 1 illustrates data for outlet flow rates of CHN03 model and Re numbers based one diameter at the boundary. The Re number is calculated by formula:

$$Re = \frac{\rho V D}{\mu} \quad (11),$$

Where ρ-blood density, V-velocity at the boundary, D-outlet diameter, μ-blood dynamic viscosity

3. Literature review

The investigation of particles' dynamics was performed by analysis of particle's trajectories via pair dispersion. Bourgoin [34] described the pair dispersion via iterative ballistic mechanism. The main idea of the proposed point was that the pairs of tracers, separated by initial distance D_0, starts to diverge ballistically. With every iteration step k, the mean square separation between the pair of particles increases from D_k^2 to D_{k+1}^2 with the growth rate $S_2(D_k)$.

The evolution of the mean square separation between particles with time is expressed through the following iterative equation:

$$D_{k+1}^2 = D_k^2 + S_2(D_k) t_k^2(D_k) \quad (12)$$

with time lag t_k, during which the mean square dispersion occurs.

It is supposed that the change of the distance between fluid elements is described by two regimes. The first regime is Batchelor regime, during which the dispersion rate grows ballistically:

$$\langle (\vec{D} - \vec{D}_0)^2 \rangle = S_2(\vec{D}_0) t^2 \quad (13)$$

where $S_2(\vec{D}_0)$ is structure function, $S_2(\vec{D}_0) = \frac{11}{3} C_2 \epsilon^{2/3} {D_0}^{2/3}$. C_2 in latter equation is a Kolmogorov constant, which equals to 2.1, and ϵ is energy dissipation rate per unit mass, dimension of which is $[m^2 s^{-3}]$).

Then, Batchelor regime is followed by Richardson regime, which is characterized by increase of mean square dispersion as t^3 [35, 36]

$$\langle (\vec{D} - \vec{D}_0)^2 \rangle = g \epsilon t^3 \quad (14)$$

where g is the Richardson constant, which is estimated to be approximately equal to 0.5-0.6.

There were attempts to describe the properties of the turbulent flow by Kolmogorov [5]. Kolmogorov [5] proposed the theory, which set the connection between Navier-Stokes equations and two experimental laws, established earlier. First law is related to phenomenon of finite energy dissipation and characterizes the behavior of the energy dissipation per unit mass for low-viscosity fluid:

$$\varepsilon = \frac{1}{2} C_D \frac{U^3}{L} \tag{15}$$

where L is reference length, U is velocity of the body and C_D is drag coefficient.

The second law connects the mean square velocity increment $\langle (\delta v(D))^2 \rangle$ with the structure function $S_2(D)$ and the separation distance between the fluid particles D:

$$S_2(D) \equiv \langle \left(\delta v(D)\right)^2 \rangle \tag{16}$$

Sawford [37] made comprehensive review, which focused mainly on modeling approaches. Sawford [37] took into consideration the specific cases of isotropic scalar fields and determined relation between them and turbulent mixing.

The review, made by Salazar and Collins [38], emphasized the empirical outcomes, acquired from field measurements, laboratory experiments and direct numerical simulations. Salazar and Collins [38] added the theory in review, which helped to interpret the experimental and numerical data, and observations into correct scope.

Boffetta and Sokolov [39] explored the statistics of two-particle dispersion in turbulent flow via the direct numerical simulations of two-dimensional turbulence. The exit time statistics at fixed scale and standard statistics at fixed time were applied during analysis of numerical results. The outcome of the research was determining value of Richardson constant in terms of diffusion equation and comparison of it with the original Richardson's description.

Biferale et al [40] investigated the pair dispersion of the tracers in the homogeneous isotropic turbulence. Biferale et al [40] conducted direct numerical simulation, which included the movement of two million tracers in time period of about three decades. The obtained Langrangian statistics of pairs of particles allowed to express particle pair trajectories as function of time and as function of distance between them. The result was the quantification of abnormal corrections to Richardson diffusion in the inertial subrange of scales.

The numerous studies were conducted on the identification of stenosis in blood arteries. The severity of artery stenosis could be identified based on implementation of anatomical and hemodynamic parameters [41]. The former one is related to implementation of computer tomography angiography (CTA) method to facilitate the identification of vessel occlusion regions. The hemodynamic approach describes the pattern of blood flow in arteries and enables to identify fractional flow reserve (FFR), which is the ratio of vessel distal pressure at stenotic region to aortic one. FFR is an invasive technique and could be quantitatively measured by placing pressure sensor across a stenotic vessel. However, invasive approach implemented during coronary angiography is not cost-effective and readily applicable. FFR is an accurate technique in medical therapy used to identify stenotic regions. The numerical value of FFR less than 0.80 indicates that the revascularization is required. As an alternative, non-invasive techniques that uses FFR based on Computational Fluid Dynamics software to quantitatively evaluate the severity of patient's CAD could be implemented [42]. Therefore, the implementation of FFR techniques, either invasive or

non-invasive, could predict the severity of CAD and diagnose the disease on the early stage to further prevent its unwanted consequences.

The mechanics of fluid interaction with particles represent complex phenomena in fluid dynamics and requires numerical methods to model the particle trajectories within the flow field. Depending on the density variations of these flow fields, particle phase can either lead or lag behind the fluid phase. The fluid flow exerts forces and moments on particles. In addition, the particle phase disturbs the continuous phase, thereby contributing to the momentum exchange with the fluid phase. These phenomena of reciprocal momentum transfer between fluid and particle phases is termed as two-way coupling. The numerical treatment of two-way coupled fluid-particle interaction ensures rigor and accurate results, being computationally expensive at the same time. As an alternative, fluid-particle interaction is resolved via one-way coupling. This method does not imply local momentum exchange between particle and flow field and treats the dynamics of each flow fields independently [43].

The hemodynamics of blood flow in vessels is governed by continuity and Navier-Stokes equations. The first one is modelled as follows:

$$\frac{\partial \rho}{\partial t} + \nabla(\rho \boldsymbol{u}) = 0, \quad (17)$$

Where ρ-fluid density, t-time and u- velocity vector

The Navier-Stokes equation is written in the following form:

$$\frac{\partial(\rho \boldsymbol{u})}{\partial t} + \nabla.(\rho \boldsymbol{u}\boldsymbol{u}) = -\nabla p + \nabla.\tau + S_{\phi}, \quad (18)$$

where p- pressure, τ- viscous stress and S_{ϕ} is the term describing body forces.

The governing equation describing the particle motion inside the artery is Maxey-Riley equation:

$$m_p \frac{dv_p}{dt} = F_p = \frac{1}{2}\rho C_D \left(\frac{\pi D_p^2}{4}\right)\left(u - v_p\right)^2 + V_p(-\nabla p + \nabla.\tau) + \frac{C_a \rho V_p}{2}\left[\frac{D\mathrm{u}}{Dt} - \frac{dv_p}{dt}\right] + \mathrm{F}_{\mathrm{contact}}, \quad (19)$$

where v_p, V_p, D_p, m_p -particle velocity, volume, diameter and mass, respectively; ρ-fluid density, C_D- drag coefficient, C_a- added mass coefficient, $\mathrm{F}_{\mathrm{contact}} -$ particle-particle contact force.

Mukherjee et al. [43] conducted study related to the investigation of embolus particle interaction with blood and vessel walls of carotid bifurcation artery via Euler-Lagrange coupled approach. The CFD simulations have been conducted by authors to resolve the dynamics of blood flow and tracks of embolic particles within carotid artery. It was investigated that the emboli particle volume fraction in the blood flow and their geometry are the main factors that affect fully coupled fluid-structure interactions.

For the small sized particles as compared to artery diameter, the implementation of one-way coupling technique is considered as a first order approximation to two-way coupling. The investigation of emboli path lines and their interaction with blood flow indicated that helicity of fluid flow is an important indicator whenever the particle trajectories within vessels are explored. In addition, apart from two-way coupled blood-particle motion, the effects of emboli particle interaction with carotid artery wall have to be taken in account to predict the regions of wall occlusion [43].

Jung et al. [44] has investigated pulsatile hemodynamics of multiphase flow in human vessel. The interaction of particulates, represented by red blood cells, with vessel walls was relevant for comprehending atherosclerosis since the plaques formation occurs on inner side of

arteries. The RBCs concentrate on the boundary layer of the outer vessel walls due to their blockage by the highly viscous central portion of curved artery with negligible shear rate in this part [44].

Kaewbumrug et al. [45] has numerically investigated the turbulent blood flow laden with dispersed bioparticle in left anterior descending (LAD) coronary artery subjected to three various wall stenosis degree severity, i.e 25%, 50% and 75%. The main findings of the studies is that the wall shear stress and pressure drop are highest in artery with the largest stenosis degree, i.e. 75%. That was validated by conducting numerical simulations in Ansys Fluent solver. In addition, the higher wall shear stress is observed in LAD artery region that has higher bioparticles concentration.

4. Methodology

4.1 Flow simulations

Simulation of turbulence flow field has been performed in OpenFOAM software. Open Foam is an open source library package for flow simulations. DNSFoam and PISOFoam solvers were used to solve DNS and LES turbulence models, respectively. Flow domain was set to cube with edge size of 2π [m], Figure 4 (a). Surface boundary conditions of 6 walls were set to triply periodic boundary conditions. Initialization of velocity and pressure fields were obtained with Taylor Green Vortex as shown in equations (20-23) [19], Figure 4 (b).

$$u_0 = U_0 \sin(x)\cos(y)\cos(z), \tag{20}$$

$$v_0 = -U_0 \cos(x)\sin(y)\cos(z), \tag{21}$$

$$w_0 = 0. \tag{22}$$

$$p_0 = p_\infty + \frac{\rho_0 U_0^2}{16}(2+\cos(2z))(\cos(2x)+\cos(2y)), \tag{23}$$

Where $U_0 = 2.5\frac{m}{s}$, $\rho_0 = 1.178\frac{kg}{m^3}$, $p_\infty = 101325\frac{N}{m^2}$

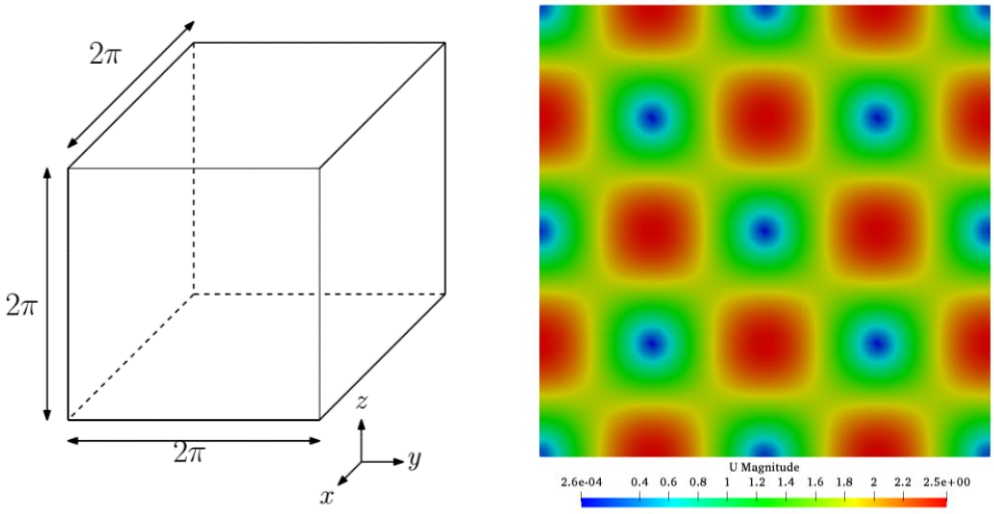

Figure 4. Mesh domain (Left) and TJV initialized velocity field at t=0 (x-y plane) (Right)

Mesh domain of 2π cube was divided into N elements in each direction, total number of mesh cells being N^3 where N = 32, 64, 128 and 256.

As it was discussed before, stochastic forcing of large-scales needs to be applied to develop not decaying HIT [21]. Equation (2) is used to add kinetic energy to specified range of

wavenumbers $k\epsilon\left[0,\sqrt{8}\right]$ which was used as forcing range of wavenumber in works of [20], [24] and [21]. Values of scales "k" are located in range of $k_{low} = \frac{2\pi}{L}$ and $k_{max} = \frac{\sqrt{2}}{3}k_0 N$.

All simulations are performed with $dt = 0.005\ s$. Pressure field and velocity data field was recorded with an intervals of 0.5 s of flow simulation time. Volume averaged velocity fluctuations are monitored with Equation (15). Integral length scale has been calculated by equation suggested by [21] as shown below (14)

$$L = \frac{\pi}{2U'^2}\int_0^{k_{max}} k^{-1}E(k)dk \tag{24}$$

U' is the RMS value of volume averaged velocity fluctuations.

$$U' = \sqrt{\frac{1}{3}(\langle U'xx\rangle + \langle U'yy\rangle + \langle U'zz\rangle)} \tag{25}$$

Average rate of energy dissipation can be estimated by (26)

$$\epsilon = \frac{U'^3}{L} \tag{26}$$

Taylor microscale is estimated with (27)

$$\lambda = \sqrt{15\frac{\nu}{\epsilon}} \tag{27}$$

Taylor scale Reynolds Number is estimated as follows (28)

$$Re_\lambda = \frac{U'\lambda}{\nu} \tag{28}$$

Kolmogorov time scale is evaluated with (29) and large eddy turnover time is estimated with (30)

$$t_\eta = \left(\frac{\nu}{\epsilon}\right)^{\frac{1}{2}} \tag{29}$$

$$T_e = \frac{L}{U'} \tag{30}$$

Main flow parameters of flow for evaluation of HIT will be U',Re_λ, L and t_η.

In addition, parallelization of mesh domain needs to be implemented to decrease the computational domain. Simple mesh decompositions methods where domain of study is divided into sliced sections are shown in Figure 5 (a). Due to presence of Fourier space in stochastic forcing term which require equal number of elements in each coordinate system, it is not possible to apply simple sliced mesh decomposition method.

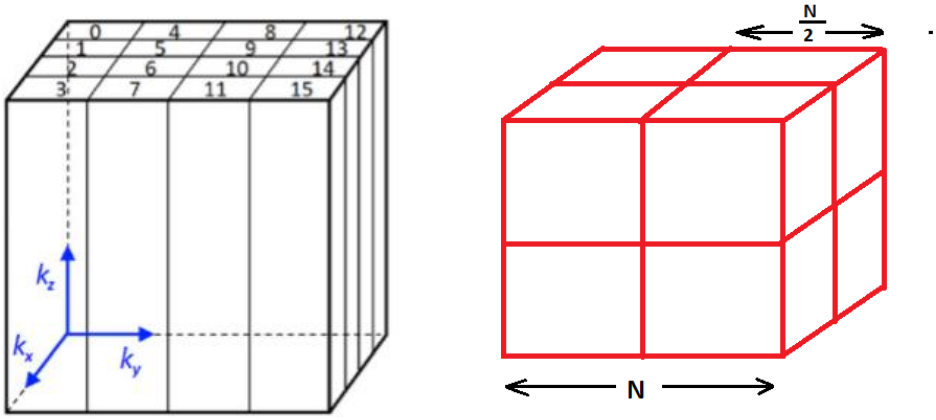

Figure 5. Simple decomposition (Left) and suggested decomposition (Right)

It was decided to divide the mesh domain into equal size cubes with number of element in each direction being half of initial grid points (N).

4.2 Simulation of particle phase

The results obtained from the flow simulation are then used for simulation of particle phase. From the energy spectrum graph, it was determined that turbulence becomes statistically stationary after about 40 seconds. The velocity field from the flow simulations after the fortieth second was used for calculation of particles' trajectories. The simulations were performed in Matlab and CFDEM.

Simulations in MATLAB

The velocity fields were imported to the Matlab. Then, the particles were inserted in the flow. Initially, the particles were inserted in a way to form a box-shape grid. The initial distribution of particles is demonstrated in figure below. The number of particles was set to 512.

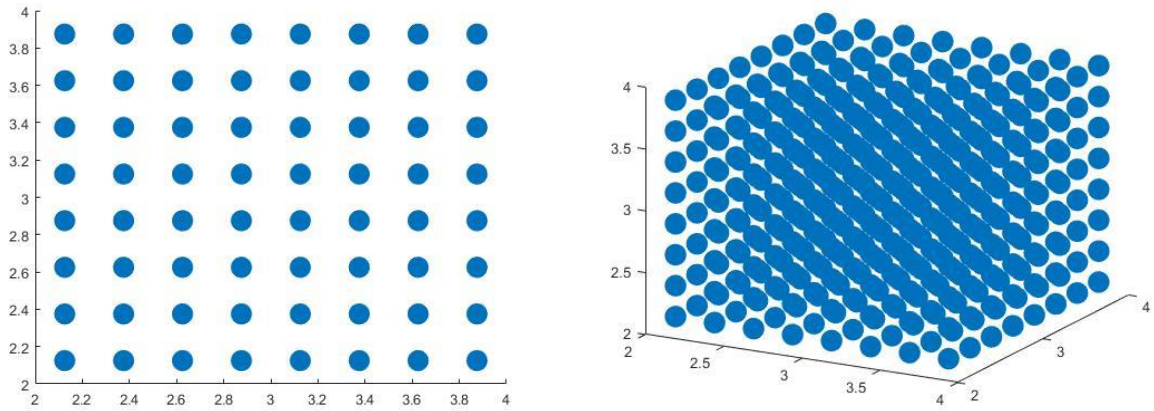

Figure 6. The initial distribution of particles in the domain front view (Left) and isometric view (Right)

Since the velocity of the flow is assigned to certain points in the domain and the coordinates of the particles differ from the coordinates of points, the velocity field was interpolated to determine the velocity of the flow in the locations of particles. Different interpolation techniques were used for interpolation including linear, nearest (assignment of the value of the nearest point), cubic. Finally, it was decided to use "Makima" technique based on third-order Hermite polynomials used by Stelzenmuller et al. [46]. The numerical differentiation was performed using the central difference method shown in (31).

$$f'(x) = \frac{f(x+h) - f(x-h)}{2h} \qquad (31)$$

The parameters used in the simulation are shown in Table 1.

Table 2. Parameters used in simulation of particles phase

Parameter	Value
St	0.1
N (number of particles)	512
E (dissipation rate)	0.0178 m^2/s^3

ν	$1.7*10^{-5}$ kg/(m·s)
τ_η	$3.09*10^{-3}$
τ_p	$3.09*10^{-4}$

Then Maxey-Riley equation was used for calculation of particles' trajectories. The initial velocity of inertial particles were set to zero. The obtained results were plotted in the domain. However, the simulations in Matlab revealed several constraints. The boundary conditions for the simulation were not periodic, since the domain was presented as a cube with walls. The results showed that the majority of particles tend to leave the flow domain. However, when they left the domain the interpolation could not be performed for such particles – the interpolation of velocity field showed error. Moreover, the particles in the simulations were presented as points rather than spheres. This representation of particles was not realistic. Finally, the simulations in Matlab were computationally expensive. This problem was not significant for small mesh grids, however, the increase of mesh grid size led to abrupt increase of computational time. Therefore, it was decided to perform the simulations of particle phase in CFDEM software.

Simulations in CFDEM

CFDEM is an open-source software, which combines OpenFOAM software and LIGGGHTS. OpenFOAM is used for simulation of flow, whereas LIGGGHTS is based on LAMMPS and used for simulation of particle phase. CFDEM does not include numerous libraries from OpenFOAM such as forcing term library and dnsFOAM solver. Meaning that it only allows simulating decaying turbulence with particles inside. The LES simulation was used to solve decaying turbulence with particles. Initially, the inertial particles were distributed randomly in the flow domain. The parameters of the turbulent flow were the same as for the homogeneous isotropic turbulence.

Table 3. The parameters used for decaying turbulence with particles in CFDEM

Parameter	Value
a	30μm
ε	0.0178 m^2/s^3
N	1000
ν	$1.7*10^{-5}$ kg/(m·s)
ρ_f	1.178 kg/m^3
ρ_d	1000 kg/m^3
τ_η	$3.09*10^{-3}$
St	0.323
τ_p	$9.981*10^{-4}$

4.3 Particles' pair dispersion

The data was threated via Matlab software. The experimental data, which was considered, was recieved from experiment, conducted by Sumbekova et al. [47]. The main aim of the experiment

was to observe the clustering phenomenon during strong turbulence. The experiment, conducted in wind tunnel, investigated the movement of water droplets, injected through its test section. The tracking of inertial particles occurred via illumination of wind tunnel by vertical laser sheet. The position of each particle was recorded on series of images, captured by high-speed camera. The one recording lasted 3.27 seconds with acquisition rate of 2600 frames per second. 19 cases with different Stokes and Taylor scale Reynolds numbers were considered during the experiment and for each case 20 movies were recorded. In total, it results to 380 movies, which were analyzed. The variation of Stokes number occurred through the change in injected water droplets' diameter and their flow rate, whereas the Reynolds number was changed via increase in wind velocity in wind tunnel. The wind velocities which were set during the experiment were 2.5 m/s, 5 m/s, 7.5 m/s and 10 m/s. All considered values of parameters and corresponding to them values of Kolmogorov time and length scales are represented on Table 4.

Table 4. The values of parameters. [9]

U(m/s)	D (mm)	F_{water} (L/min)	η (μm)	τ_η (s)	$St_{D_{max}}$	Re_λ
2.5	0.3	0.8	431	0.011	0.3	200
5.0	0.3	0.8	250	0.004	0.7	300
7.5	0.3	0.8	162	0.002	1	400
10.0	0.3	0.8	114	0.001	5	490
2.5	0.3	1.2	429	0.011	0.1	240
5.0	0.3	1.2	255	0.004	0.5	350
7.5	0.3	1.2	174	0.002	0.9	390
10.0	0.3	1.2	118	0.001	2.7	470
2.5	0.4	1.9	439	0.012	0.3	240
5.0	0.4	1.9	260	0.004	1.4	290
7.5	0.4	1.9	174	0.002	1.6	420
10.0	0.4	1.9	121	0.001	2.8	480
5.0	0.4	1.43	252	0.004	0.5	300
7.5	0.4	1.43	166	0.002	1.4	420
10.0	0.4	1.43	118	0.001	2.7	480
2.5	0.5	1.9	442	0.012	0.1	200
5.0	0.5	1.9	249	0.004	0.8	290
7.5	0.5	1.9	168	0.002	2.3	400
10.0	0.5	1.9	120	0.001	3.5	480

The detected positions of the water droplets were processed and the coordinates of particles on each image were determined. The Matlab code sorted inertial particles by all possible combinations of pairs. For each pair the square of distance between the particles was calculated. Mean square dispersion and its evolution with time for each set of measurements were obtained. The mean square separation was normalized by the dissipative scale η^2 , whereas time was normalized by the dissipative time scale τ_η. The number of graphs, representing the dependence of mean square dispersion on normalized time, was constructed.

4.4.1 Simulations of particles (blood clots) in arteries

The numerical simulations of two-phase flows in coronary arteries have been performed via Ansys Fluent finite-element solver. The Ansys CFD software enables to discretize and numerically solve continuity and Navier-Stokes equations. The blood was treated as non-Newtonian, incompressible, steady fluid with density 1060 kg/m^3 and dynamic viscosity of 0.0035 m^2/s. The blood clots were modelled as spherical particles with density 1100 kg/m^3 and dimeter of 2.5 mm. (Romero, 2013). The artery wall density was set to 1160 kg/m^3. After the 3D geometry has been imported in Ansys solver, the mesh was generated. In order to validate the independence of results from the grid size, the mesh independence study has been conducted, which is described in the following section. The blood phase and particle phase, represented by blood clots, were resolved using one-way coupled Euler-Lagrange approach. As Indicated in Table 1, the flow regime was laminar throughout the CHN03 artery. In the 'Setup' mode, the 'Viscous' model has been chosen. The thermodynamic properties of blood, clots and artery wall, i.e. density and viscosity, has been typed in 'Materials' section. In 'Cell Zone Conditions' mode, the fluid type has been changed from solid to liquid. In the 'Boundary Conditions' windows, the pressure and mass flow rate were assigned for inlet and outlets, respectively. The mass flow rate at the outlets has been calculated by multiplying blood density by the volume flow rate. In the 'Solutions Methods' mode, the 'Coupled' scheme has been selected for pressure-velocity coupling. The 'Least Squares Cell Based' gradient has been selected for spatial discretization. The pressure and momentum equations were discretized with 'Second Order' and 'Second Order Upwind' Scheme. The Discrete Phase Model has been tuned on to inject particles at the inlet and track their motion within artery. The particle phase was tracked in a steady mode. Initially, 100 particles were injected at the inlet of vessel of CHN03 model. Firstly, the single blood flow phase was simulated with 1000 iterations to attain fully developed entrance region in laminar flow field and reach the statistical convergence of the velocity profiles. Afterwards, the two-phase flow field was injected until further convergence within the defined tolerance. In total, 8000 iterations were performed for CHN03 model. The convergence criterion was set to residual values of 10^{-6} for each parameter, i.e. continuity and x, y, z velocity equations.

4.4.2 Mesh convergence study

The mesh convergence study has been conducted for CHN03 model in order to validate the independence of results on the variation of element size. The computational domain of the artery 3D geometry has been discretized into finite elements to ensure accurate numerical results. The mesh of tetrahedral structure has been assigned for the curved vessel geometry. Table 5 illustrates the variation of parameters, i.e. average and maximum velocities and pressure, against number of mesh nodes and elements variation. The parameters that were selected for the variation against number of elements are maximum pressure and maximum velocity. Table 6 illustrates that the percentage error of maximum pressure and velocity between consecutive iterations is equal to

0.164% and 0.966%, respectively. That is reasonable estimate since the difference between results is less than 1%.

Table 5. Variation of parameters against mesh size

#	P1 - Mesh Element Size [mm]	P2 - Mesh Nodes	P3 - Mesh Elements	P4 - vel_average [m s^-1]	P5 - pressure_average [Pa]	P6 - max pressure [Pa]	P7 - max_vel [m s^-1]
1	0.06	2053486	1207306	0.218	8539.442	10211.8	2.484
2	0.08	1691078	984306	0.239	8543.102	10213.0	2.502
3	0.10	1293550	753515	0.257	8537.293	10215.7	2.456
4	0.13	959461	557157	0.276	8541.524	10199.0	2.480
5	0.16	785319	454797	0.290	8563.695	10214.1	2.417
6	0.20	586597	338118	0.309	8577.951	10186.6	2.384
7	0.25	476578	273537	0.324	8596.220	10197.0	2.364
8	0.30	407065	232110	0.335	8616.228	10203.6	2.432
9	0.35	394947	225366	0.337	8612.335	10208.9	2.383
10	0.40	320016	183246	0.353	8618.041	10209.0	2.324
11	0.45	266321	152203	0.364	8676.891	10212.3	2.341
12	0.50	244711	139474	0.366	8688.774	10201.1	2.313
13	0.60	183284	103494	0.379	8773.333	10237.8	2.215

Table 6. Percentage error between consecutive iterations on maximum velocity and pressure

No. of mesh Elements	Max pressure, Pa	% Error of Pmax	Max velocity, m/s	%Error on Vmax, m/s
103494	10237.8	-	2.215	-
139474	10201.1	0.3581	2.313	4.428
152203	10212.3	0.1094	2.341	1.196
183246	10209.0	0.0324	2.324	0.703
225366	10208.9	0.0010	2.383	2.509
232110	10203.6	0.0516	2.432	2.050
273537	10197.0	0.0651	2.364	2.793
338118	10186.6	0.1019	2.384	0.877
454797	10214.1	0.2701	2.417	1.369
557157	10199.0	0.1480	2.480	2.594
753515	10215.7	0.1642	2.456	0.966
984306	10213.0	0.0268	2.502	1.895
1207306	10211.8	0.0117	2.484	0.740

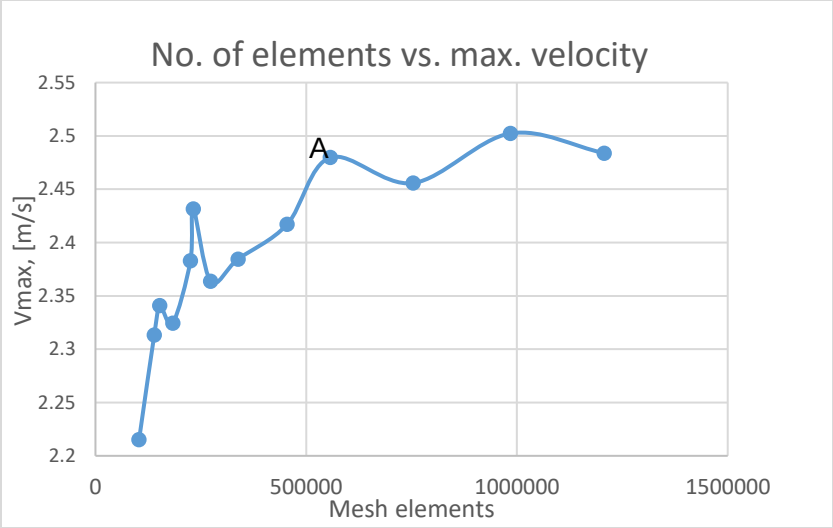

Figure 7. The dependence of maximum velocity on the number of mesh elements

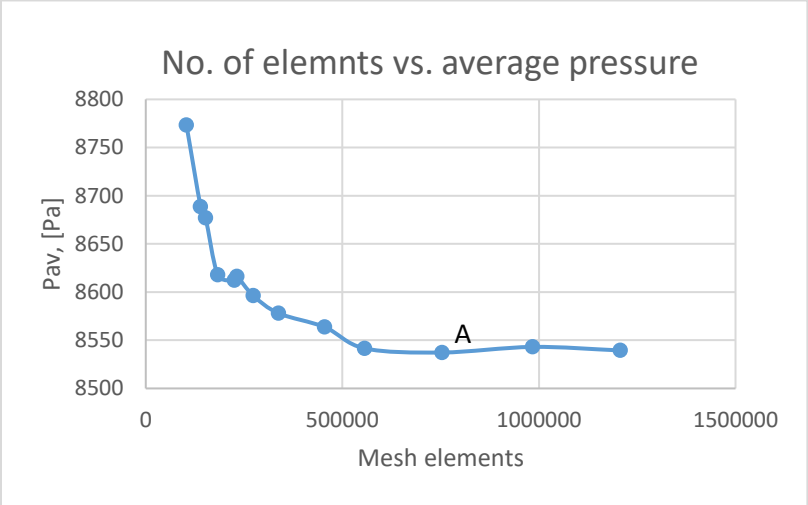

Figure 8. The dependence of averaged pressure on the number of mesh elements

Figure 7 and 8 depicts the variation of maximum velocity and average pressure parameters against number of mesh elements. It is observed that after the vicinity of point A has been reached, the variation of parameters is minor with progressively increased elements number. Therefore, the optimal mesh used for study and numerical simulations was mesh #3 in Figure 7 with 753,515 elements and 1,293,550 nodes.

4.5 Experimental part

The preliminary experiment was conducted for small sized particles of smoke. The equipment used in experiment was smoke generator, Chronos 1.4 High-speed camera and light source. The experimental setup is demonstrated in figure below.

Figure 9. Experimental setup used for tracking of small particles of smoke

Initially, camera was calibrated and placed on focus distance in front of smoke generator. The light source was placed perpendicularly to the smoke generator. The first frame was recorded without launching smoke generator in order to obtain reference frame. Then, high speed camera recorded the smoke coming out from smoke generator. Then the video taken for two seconds was divided on frames and imported in Matlab for image intensity analysis of smoke. The image intensity analysis was performed by comparison of each frame in Matlab to the reference frame. Experimental procedure was set up so to eliminate shadows of disturbances in camera view. Only disturbance source present in region of camera view is smoke generated by machine. Therefore, intensity of each frame being recorded will be changed when smoke travels through region of camera view. MATLAB code records the intensity difference between reference frame and frame at some time evolutions. Each frame contains matrix size of M where each element shows grayscale value of pixel from 0 to 255.

$$M = \begin{bmatrix} 1 & \cdots & 1280 \\ \vdots & \ddots & \vdots \\ 1000 & \cdots & 1280 \end{bmatrix} \quad (32)$$

Table 7. Image intensity analysis

Time	0	1	2	3	…	n
	M_{ref}	M_1	M_2	M_3		M_n
M_{diff}	0	$M_1 - M_{ref}$	$M_2 - M_{ref}$	$M_2 - M_{ref}$		$M_n - M_{ref}$

Each M_{diff} matrix at some ‘t” is cleared from noise and only smoke detected region coordinates are saved. This procedure identifies smoke detected regions in camera view.

5. Results and discussion

5.1 Simulation of flow

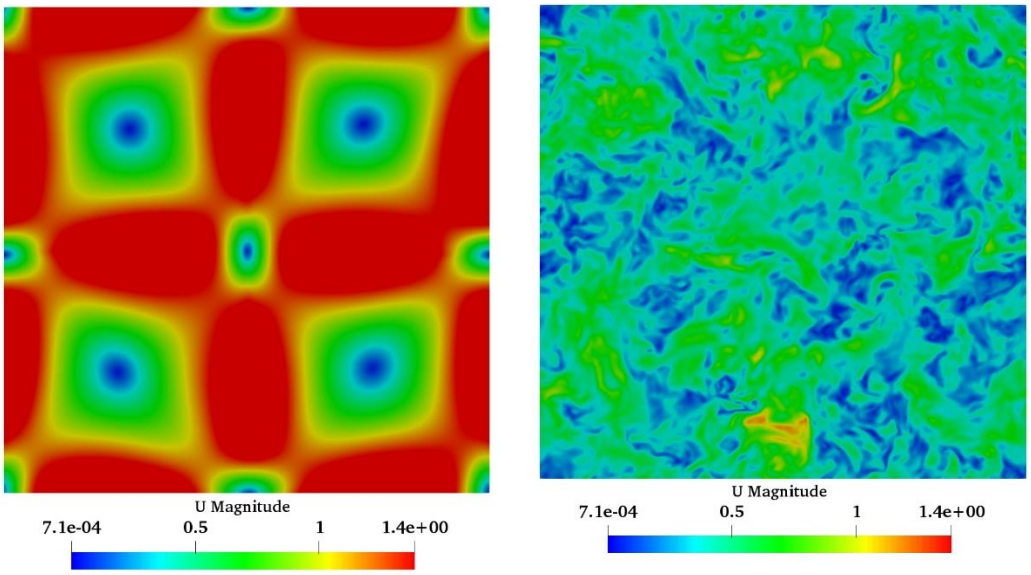

Figure 10 TJV initialized velocity field at time =1s (Left) and Velocity field at time = 26 s, N=128 (Right)

TGV initialized field with velocity amplitude of 2 m/s will decay with time evolution. Figure 10 shows velocity field at the t = 1s of simulation from LES solver for mesh size of N=256 (σ=2, α=50). Figure 10 shows velocity of HIT at t = 26 s where fluctuations of velocity field are clearly seen. These velocity fluctuations will be estimated with equation (25) and energy present in each scale will be evaluated with Energy spectrum plots, Figure 13.

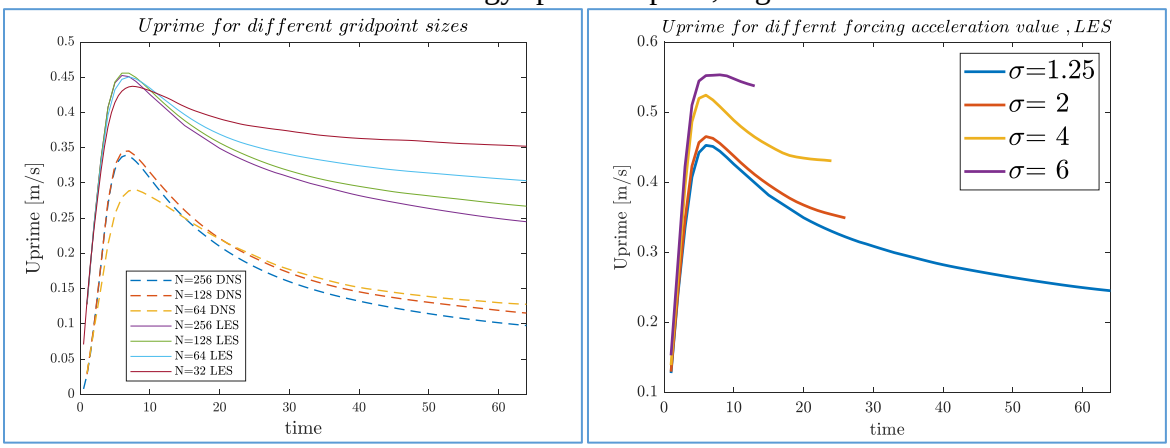

Figure 11 Mesh variation study for LES and DNS solvers (Left) time evolution of U' for different values of acceleration variance, N=256 (LES) solver (Right)

It is important to study the effect of mesh resolution on flow characteristics of simulated HIT. Mesh value of studied domain was increased gradually from N=32 until N=256. U' value was evaluated at the end time of 64s. Minimum difference of 9.0%, between consecutive values of U' for each N change, was achieved with LES solver Figure 11. DNS solver also have shown similar performance on mesh size variation, Figure 11. Minimum value of U' keeps decreasing

with increasing mesh size for DNS solution. This trend is explained with the fact that DNS is better at resolving small scales.

It is possible to increase mesh size of N to 512. Since solution was performed on a single core, intolerable increase of computational time for mesh generation at N=512 was observed. Therefore, N=256 was taken as best grid resolution for rest of calculations.

As it was discussed before, forcing term is added to achieve statistically stationary HIT. Different values of σ were simulated with LES solver for N=256. Increase in peak value of U' at turbulence generation region is observed in Figure 11. Results of this simulations show that it is possible to control values velocity fluctuations and energy dissipation rate (they are related with 26) for HIT by changing the value of acceleration variance (σ).

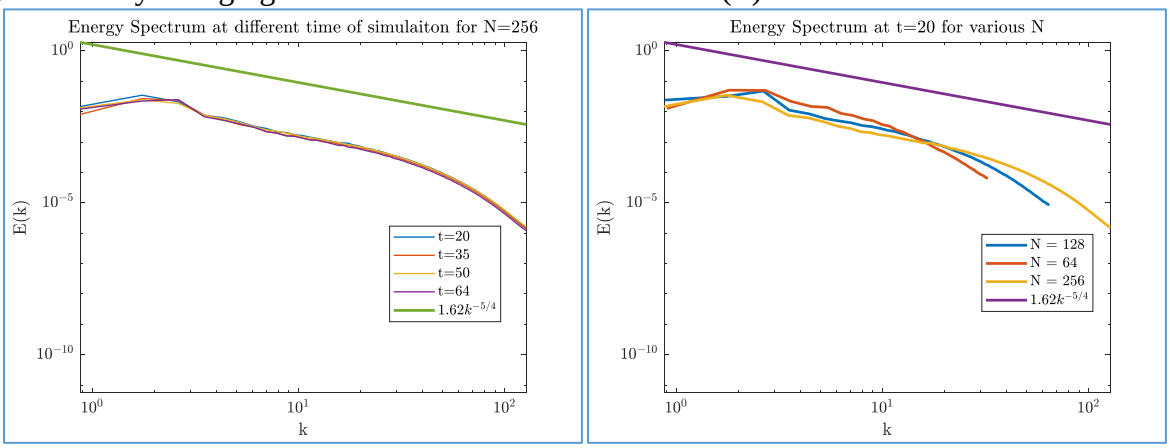

Figure 12. Energy spectrum evolution with time (Left) and energy spectrum for different grid resolution after turbulence generation is achieved (Right)

Energy spectrum is one of the main characteristics to evaluate properties of not decaying HIT. Figure 12 (Left) depicts that energy spectrum did not change with time evolution. It is supported with Figure 12 (Right) where turbulence generation is achieved approximately at t=20 s. Therefore, it is possible to state that not decaying HIT condition is expected after this time point.

The slope of energy spectrum should be close to the curve of $1.62k^{-5/4}$[20], Figure 1. It shows whether small scales are fully resolved or not. The curvature obtained by [20] cannot be fully followed since [20] has used different forcing values and forcing time in their simulations. Figure 12 (Left) shows that scales in range of $k \in [0,22]$ are fully resolved. If slope is checked after this range, the deviation from expected slope can be noticed. Figure 12 (Right) depicts energy spectrum of different grid resolutions at t = 20s. It is evident from the graph that N=256 performance is better than other two. Greater mesh resolution will capture a greater amount of small scale fluctuations. Range of wavenumber that are fully resolved is bigger for larger N as it was expected.

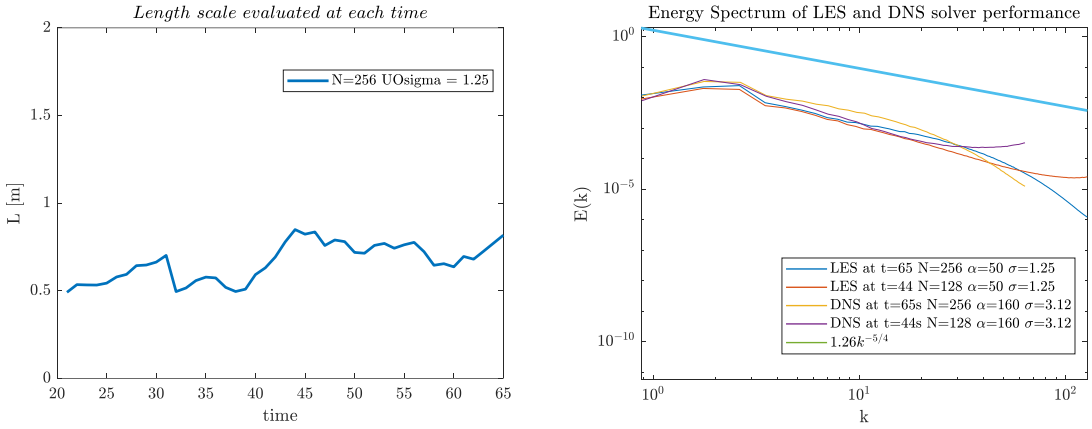

Figure 13. Estimated Length Scale variation with time after turbulence generation region (t> 20s) (b) Energy spectrum from LES and DNS solvers

Length Scale is estimated at each time step value using (24) and obtained results are shown in Figure 13 (Left). Moderate level of fluctuations is observed for length values over time. It may occur due to the presence of acceleration variance in forcing term which is based on noise producing equations. In addition, increasing trend in length scale values is observed. It can be explained with Figure 11 (Left) where U' value decreases over time which results in larger length scale values as it is stated in equation (24).

LES and DNS solver performances differ in smaller scales. DNS solver can resolve smaller scales from its definition. It can be illustrated in Figure 13 (Right) where energy spectrum curve for DNS solver for N=128 and N=256 keeps its slope close to expected curvature of energy spectrum suggested by [20].

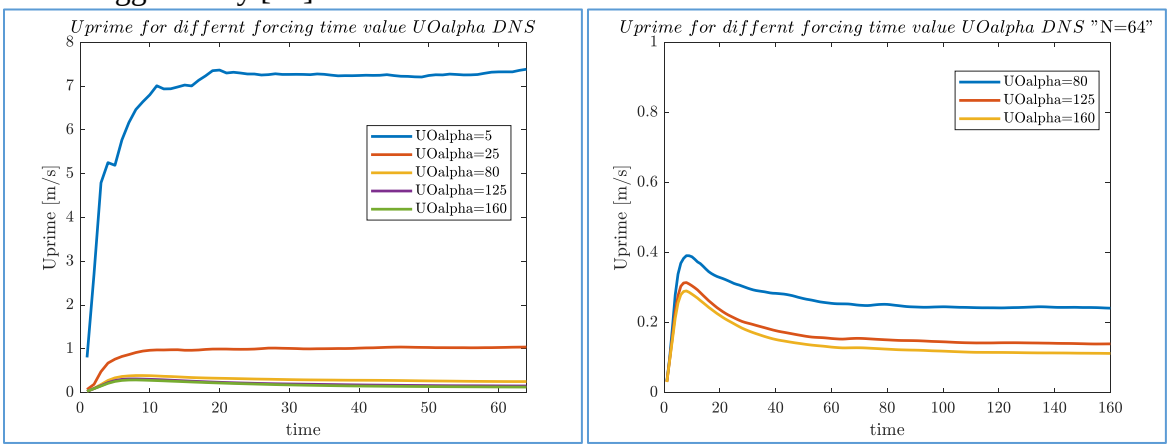

Figure 14. Effect of forcing time on U' (Left) and effect of forcing time on U' zoomed to smaller forcing time legends (Right)

Forcing time is crucial when evaluating the HIT parameters [24]. Some studies have found relation between forcing time scale and large eddy turnover time as it was noted before [25]. There are should be limit when forcing time will not have significant effect on HIT parameters like U'. Figure 14 (Left) shows that α = {80, 125, 150} are closely located which implies presence of smaller variation between U' values between the lines. Figure 14 (Right) illustrates that smaller difference is present between U' values for α = {125, 150}.

The results of N=256 simulations could not be obtained for longer simulation time due to expensive computational time consumption. Table 8 presents estimation of flow parameters at the end time of available results for N=256.

Table 8. HIT flow characteristics at the time of LES simulations

σ [m/s^2]	1.25	2	4	6
$t_{simulation}$	65	26	24	13
U' [m/s]	0.2440	0.3489	0.4304	0.5373
L [m]	0.8173	1.2629	1.8160	1.6711
ϵ [m^2/s^3]	0.0178	0.0336	0.0439	0.0928
α [1/s]	50	50	50	50
t_f [s]	0.02	0.02	0.02	0.02
t_η [s]	0.0309	0.0225	0.0197	0.0135
T_e [s]	3.35	3.62	4.22	3.11
λ [m]	0.0292	0.0304	0.0328	0.0282
Re_λ	419	624	830	890

Kolmogorov time scale (t_η) for σ=1.25 is greater than given t_f at time = 65 s. This time point is located far from turbulence generation region in Figure 11. In addition, length-scale variations are tolerable at this time point, Figure 11. Therefore, it is possible state statistically stationary flow condition is achieved.

However, t_f is greater than t_η for σ = 2, 4 and 6. Re_λ numbers are significantly large compared to σ =1.25. The results are obtained close to turbulence generation region for these mentioned values of σ = {2, 4, 6}. If these parameters will be evaluated for longer time evolution of flow for σ = {2, 4, 6}, it will be possible satisfy $t_f < t_\eta$ condition suggested by [20].

Table 9. HIT flow characteristics evaluated close to turbulence generation region, t = 13s

σ [m/s^2]	1.25	2	4	6
$t_{simulation}$	15	13	13	13
U' [m/s]	0.3814	0.4108	0.4643	0.5373
L [m]	0.4252	0.4860	0.9906	1.6711
ϵ [m^2/s^3]	0.1305	0.1426	0.1011	0.0928
α [1/s]	50	50	50	50
Tf [s]	0.02	0.02	0.02	0.02
T_η [s]	0.0114	0.0109	0.0130	0.0135
T_e [s]	1.11	1.18	2.13	3.11
λ [m]	0.0169	0.0174	0.0233	0.0282
Re_λ	378	420	637	890

Above shown Table 9 presents parameters evaluated at t = 13 s for σ = 2, 4 and 6. Re_λ and L values are scalable with acceleration variance of stochastic forcing. Larger values of σ means more energy is added to larger-scales which results in larger L and λ. However, these values are going to be stabilized when not decaying HIT will be reached.

Table 10. Computational time per simulation type

N	Total N	Average computing per time step [s]	Hours required to simulate LES/DNS solver for t=80 s
32	32768	0.108	0.48

64	262144	2	8.89
128	2097152	20.7	92.00
256	16777216	325.3	1445.78

As above shown Table 10 illustrates computation time required for N=256 is significantly large. Therefore, parallelization parallel computing approaches need to be implemented. Mesh domain decomposition method is suggested for this kind of simulation. Suggested mesh decomposition method in Figure 5 has been tested for N =64 and128 with OpenFOAM DNS solver. They were compared to single core solved simulation results and obtained values of U' were identical, Figure 15

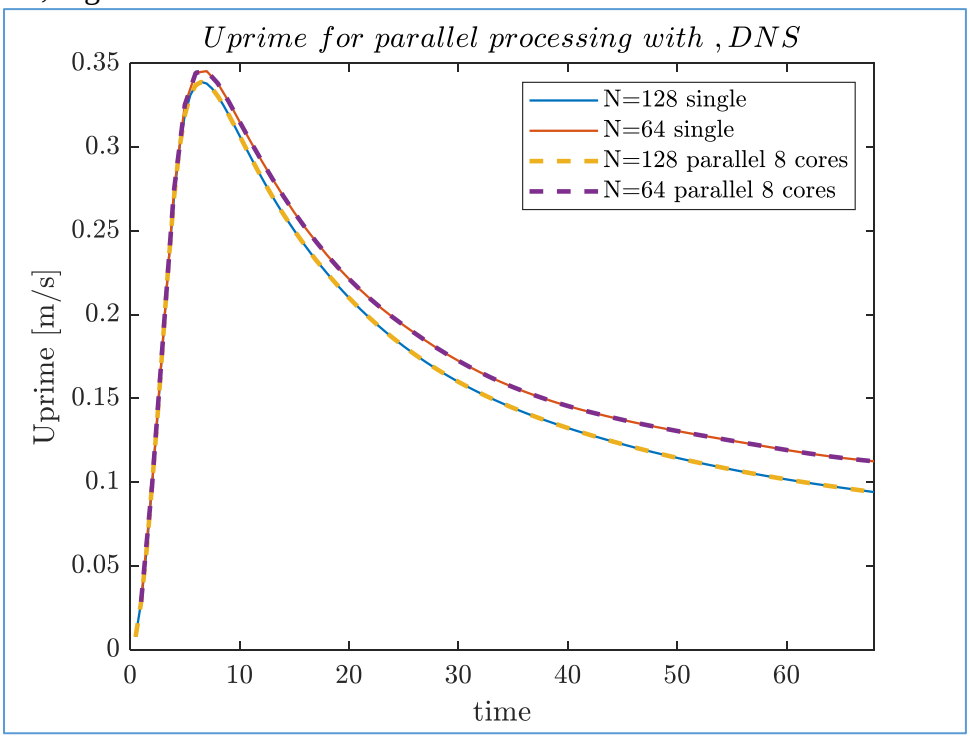

Figure 15. Parallel and single core simulation results

5.2 Simulation of particle phase

5.2.1 MATLAB Software

The results obtained in Matlab are shown in figure below.

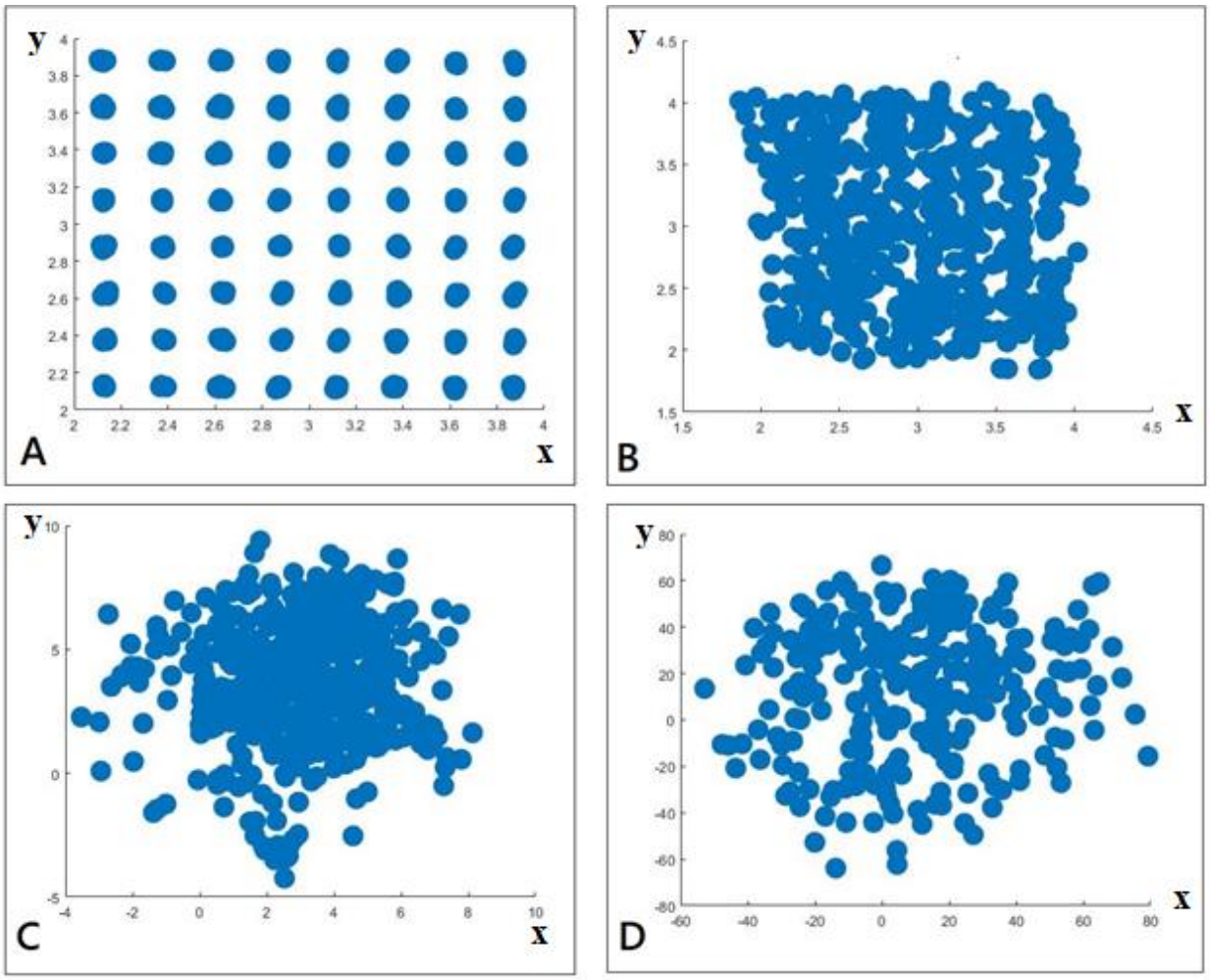

Figure 16. The distribution of particles in the space after (A) t=0.01s, (B) t=0.02s, (C) t=0.03s, (D) t=0.04s

The results obtained from MATLAB showed that the majority of particles leave the domain. For the particles, which left the domain, the interpolation was done incorrectly. The velocities of such particles were too high, therefore, their location in 0.04 seconds reached 80 meters from the initial positions. It can be seen from Figure 9 (D), that the particles are distributed in the area [-70; 70] in x-axis and [-50; 80] in y-axis. The dynamics of particles could not be investigated, since the particles were out of the flow domain and were not exposed to the influence of the turbulence. Therefore, it was decided to perform the simulations of particles phase in CFDEM software.

5.2.2 CFDEM

The results obtained for pressure and velocity fields in CFDEM are shown in figures below. The initial distribution of particles in the domain is shown in figure 10.

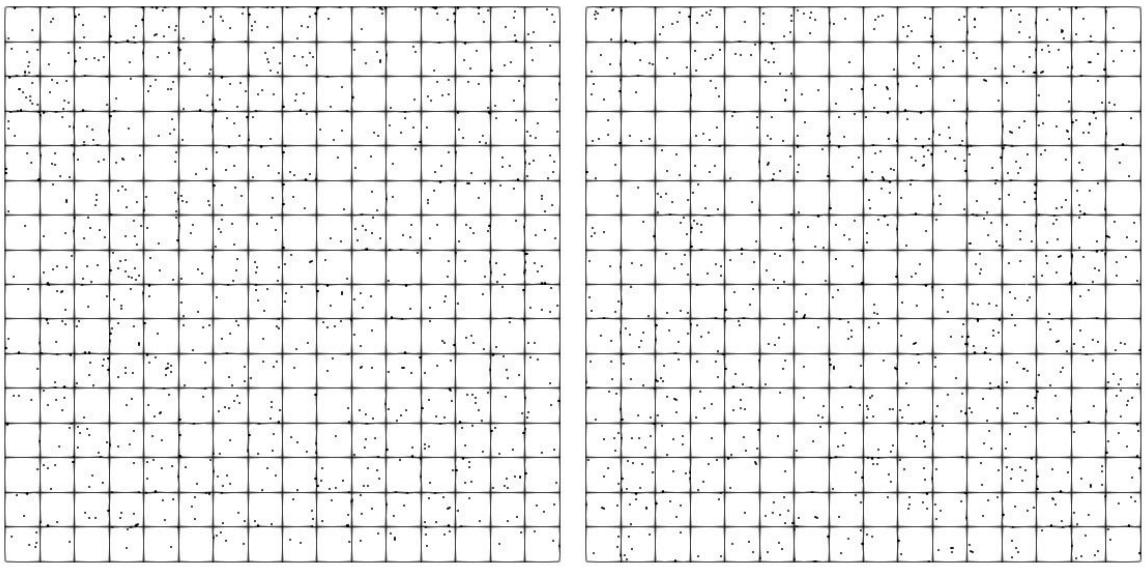

Figure 17. The initial distribution of particles in XY plane (Left) and XZ plane (Right)

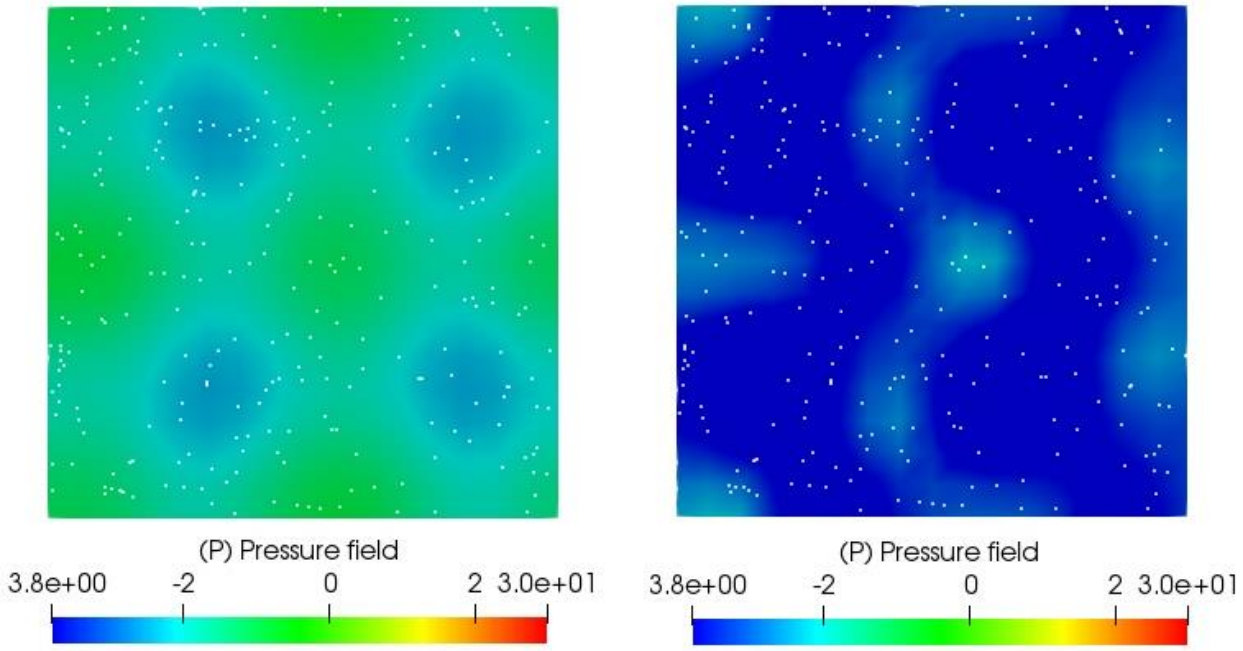

Figure 18. Pressure field obtained from decaying turbulent simulations in CFDEM. T = 0s (Left), T = 0.05s (Right)

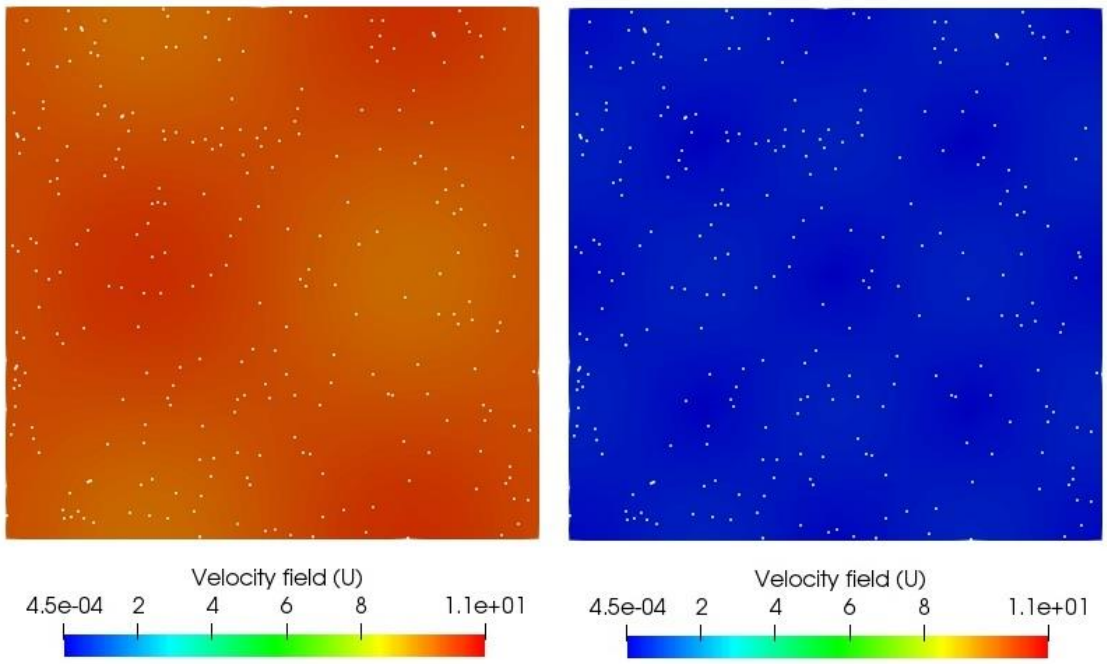

Figure 19. Velocity field obtained from decaying turbulent simulations in CFDEM. T = 0s (Left), T = 0.05s (Right)

It can be seen from Figures 11 and 12, that the turbulent flow is decaying with time. Since the boundary conditions were set to periodic, particles did not leave the flow domain and were moving in turbulent flow. However, the particle phase was simulated for only 0.05s, since the turbulent decayed.

5.3 Pair dispersion of inertial particles in turbulent flow

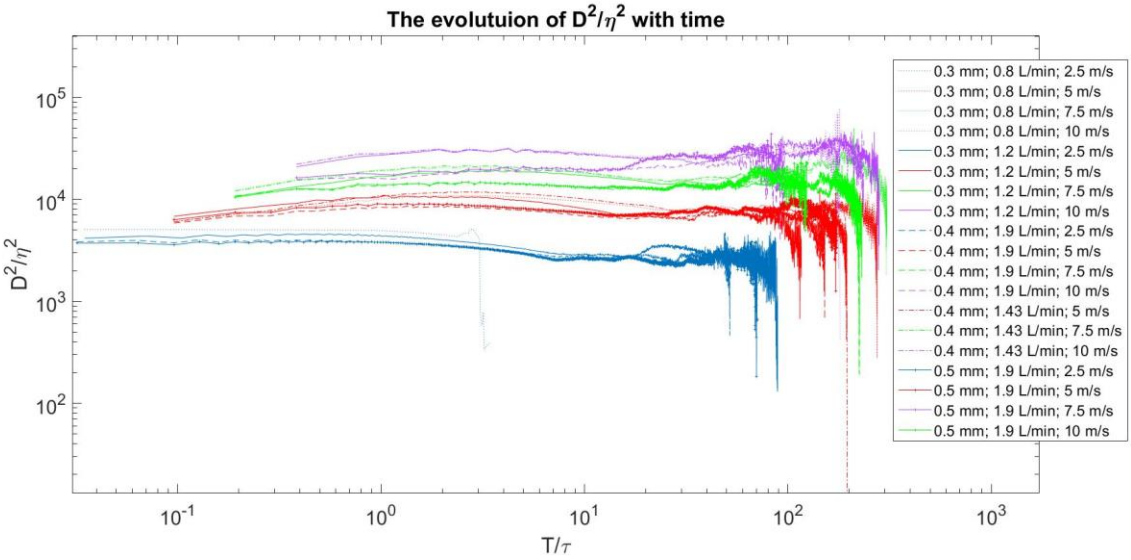

Figure 19. The evolution of mean square separation with time for all cases

The Figure 19 represents the evolution of normalized value of mean square separation with normalized time. The Figure 19 includes the results, obtained for the inertial particles for all considered cases. Figure 20-23 show same graphs for each value of wind velocity separately. All pairs of particles, initial distance between which was not exceed 100η, were considered during construction of graph. All graphs, made for the inertial particles, possess same feature. Normalized mean square dispersion does not change significantly with time during first decade. In the second half of graphs, the strong fluctuations, which are result of scarcity of experimental data, are observed. Another important point is that the higher velocity of the wind corresponds to greater value of initial separation between particles. Hence, there is correlation between velocity of tracers and initial separation value of inertial particles.

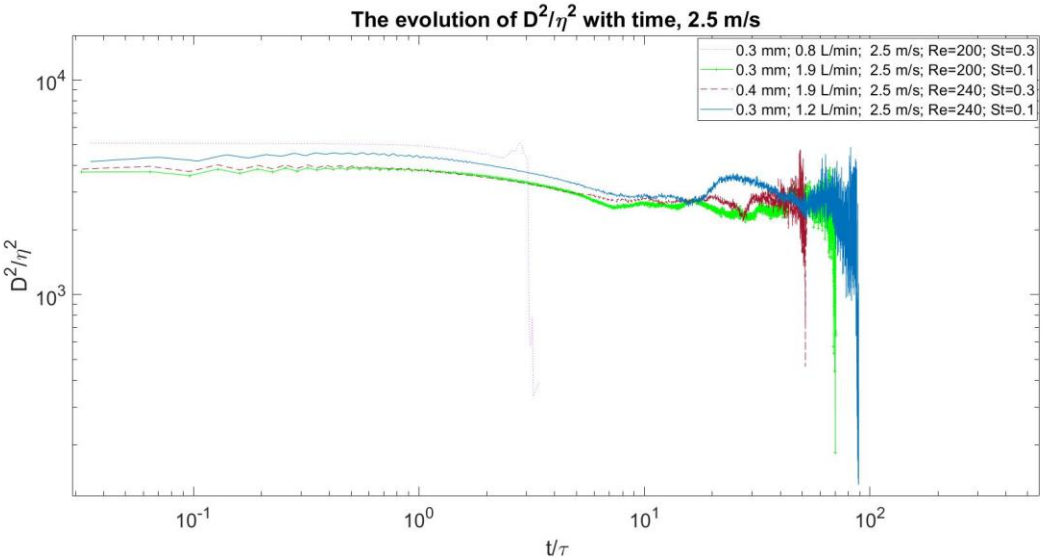

Figure 20. The evolution of mean square separation with time for wind veclocity of 2.5 m/s

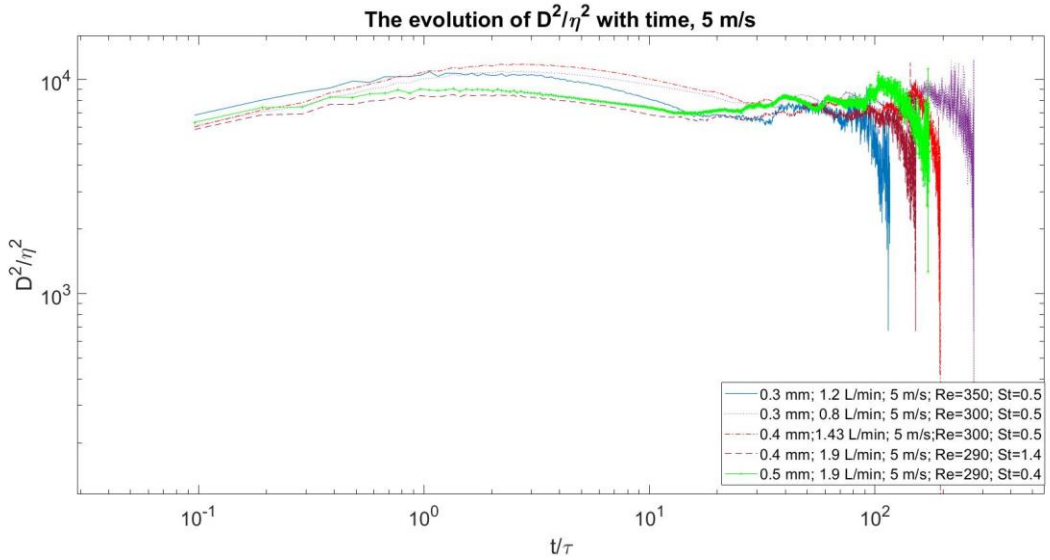

Figure 21. The evolution of mean square separation with time for wind velocity of 5 m/s

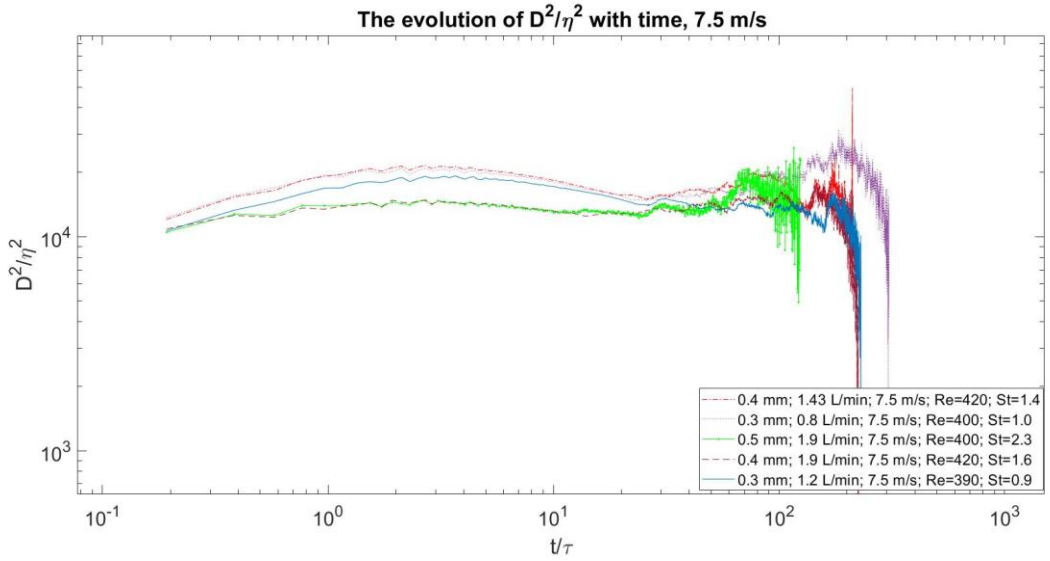

Figure 22. The evolution of mean square separation with time for wind veclocity of 7.5 m/s

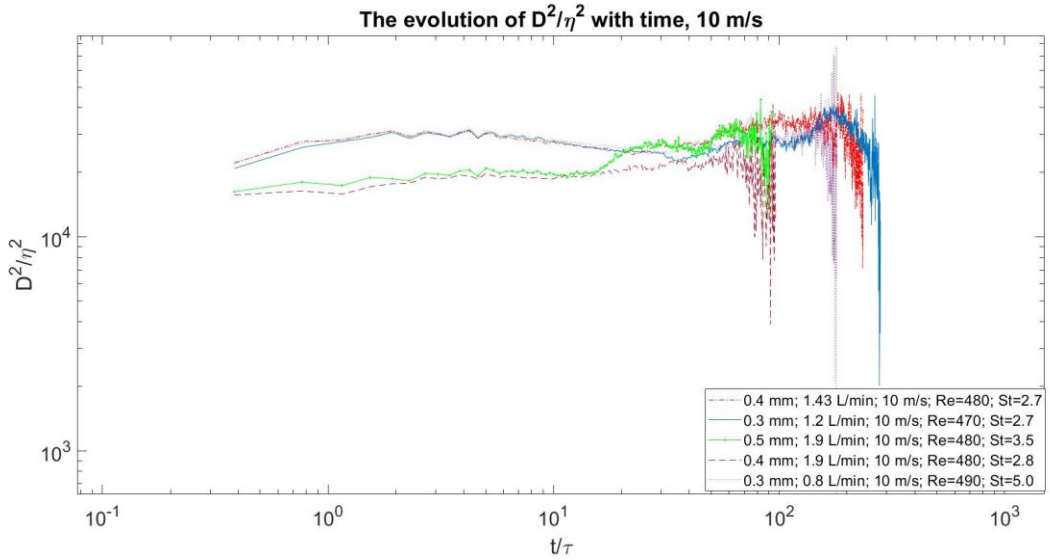

Figure 23. The evolution of mean square separation with time for wind veclocity of 10 m/s

5.4 Multiphase in coronary arteries

5.4.1 CHN03 model with 100 injected particles

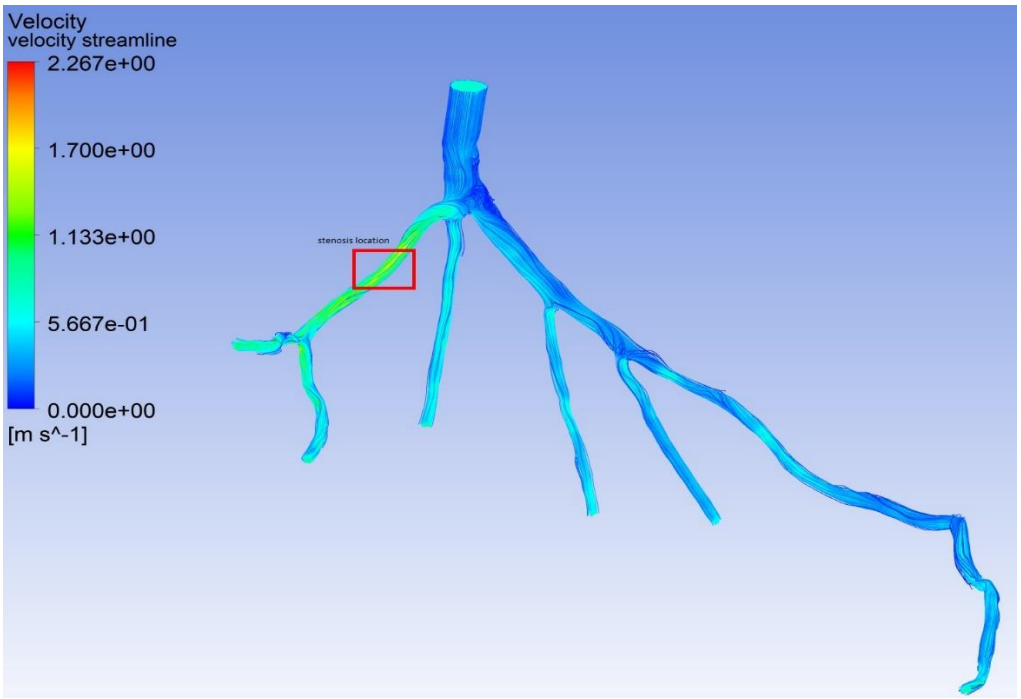

Figure 24. Velocity streamlines for CHN03 model

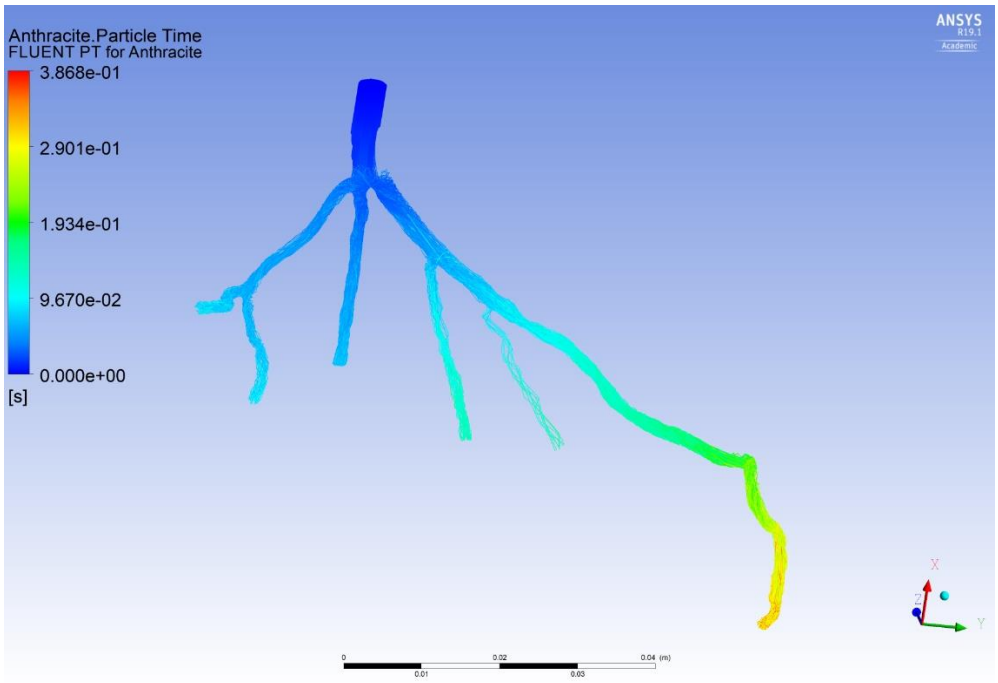

Figure 25. Particle time for CHN03 model

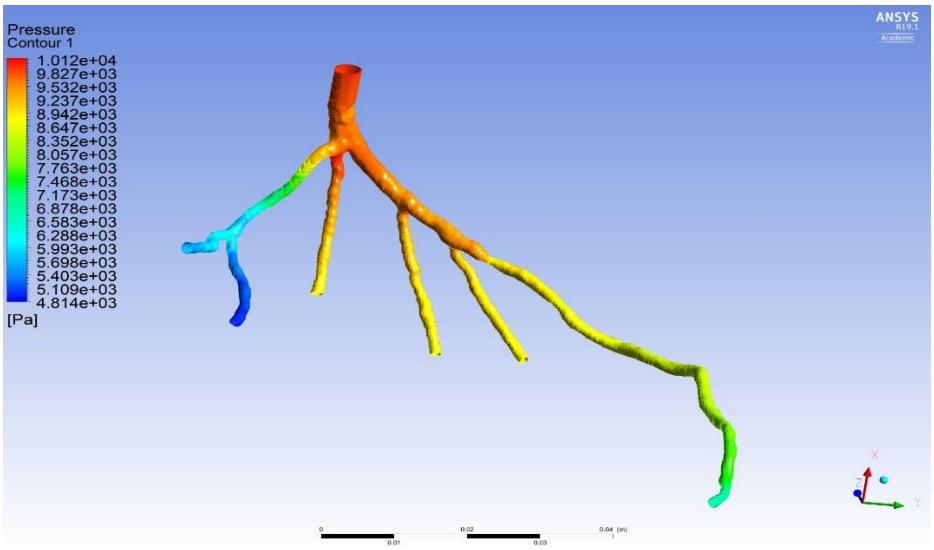

Figure 26. Pressure Contour for CHN03 model

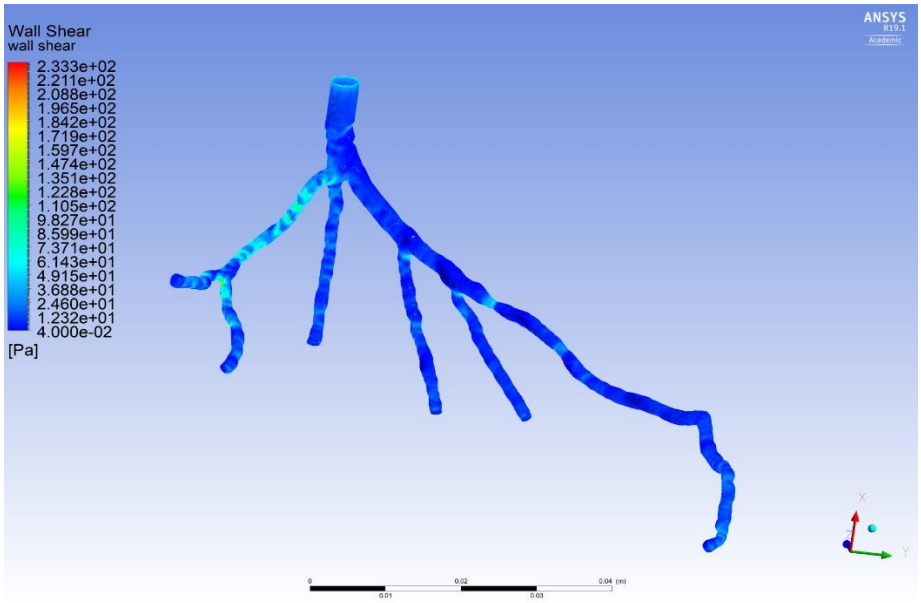

Figure 27. Wall Shear Stress for CHN03

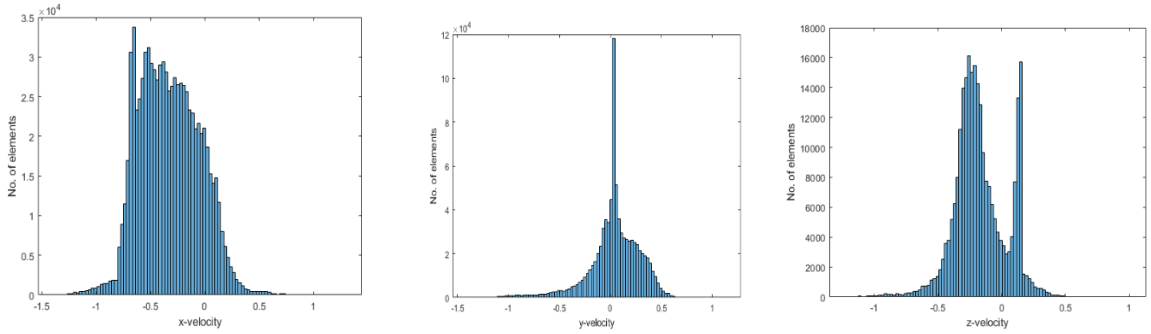

Figure 28. PDF distribution of particles (Left) x-velocity; (Central) y-velocity; (Right) z-velocity

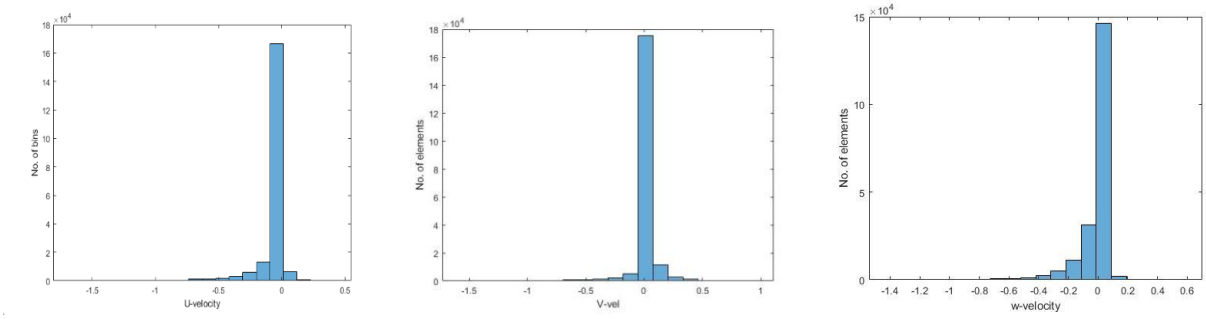

Figure 29. PDF distribution of flow (Left) x-velocity; (Central) y-velocity; (Right) z-velocity

5.4.2 CHN03 model with 1000 injected particles

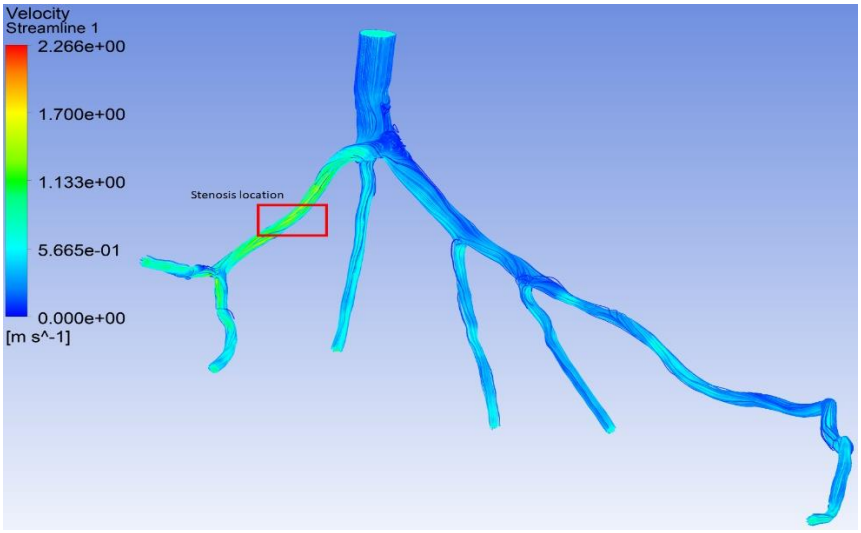

Figure 30. Velocity streamlines for CHN03 model (1000 particles)

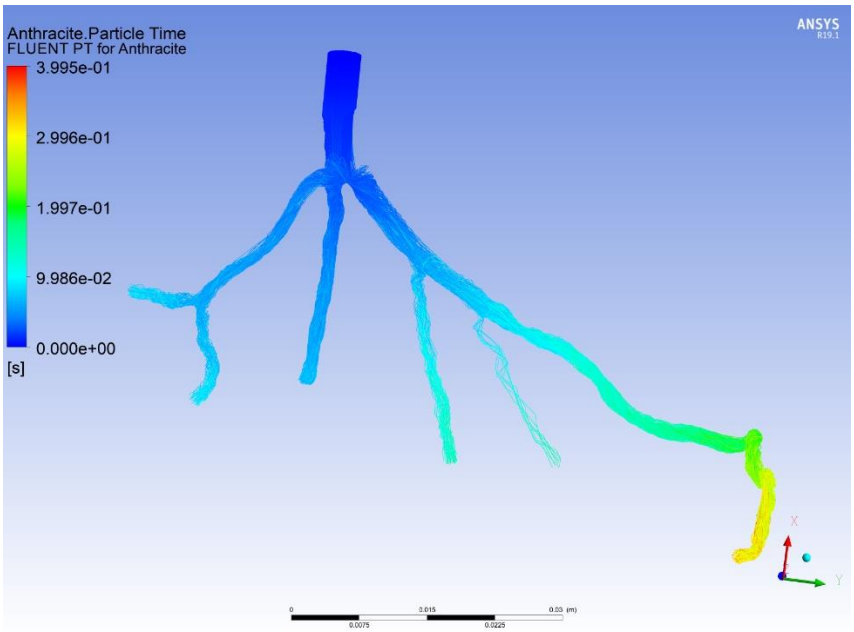

Figure 31. Particle time for CHN03 model (1000 particles)

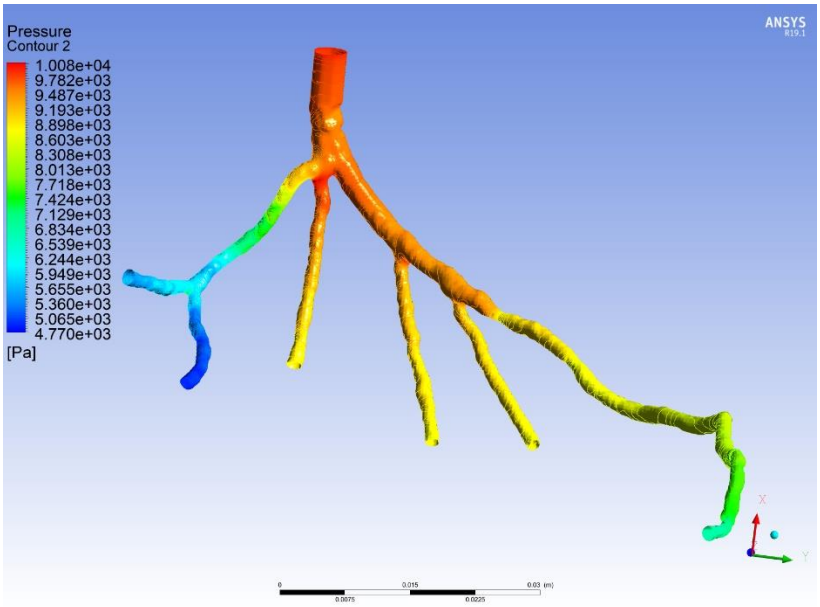

Figure 32. Pressure Contour for CHN03 model (1000 particles)

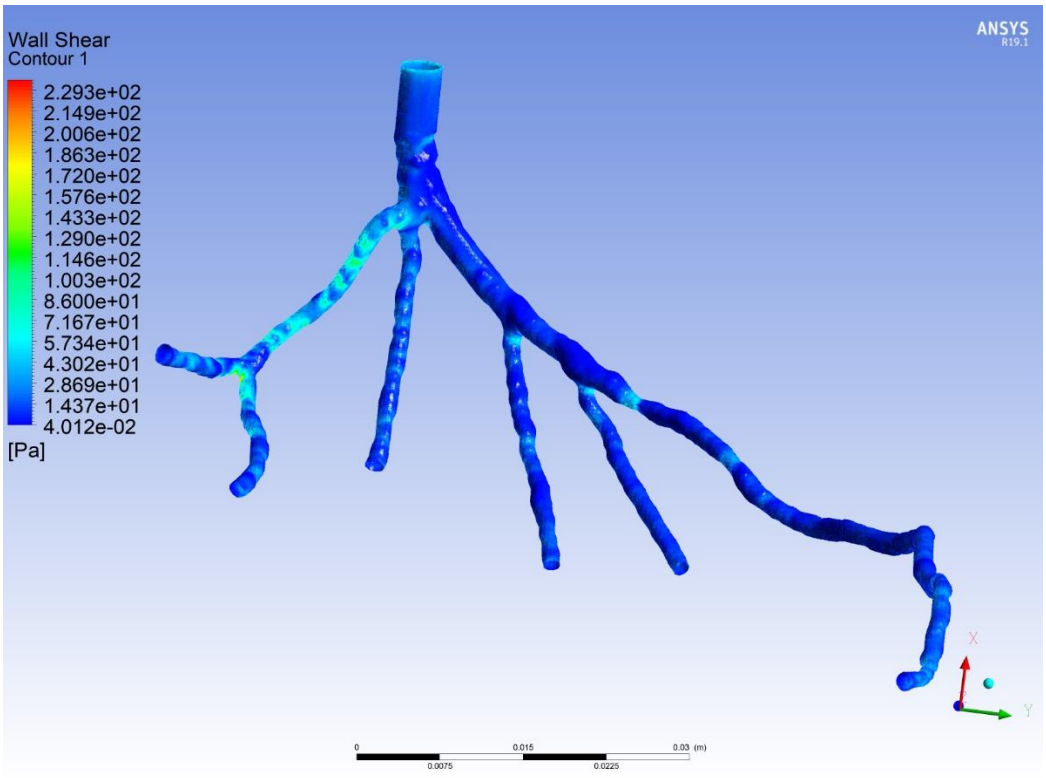

Figure 33. Wall Shear contour for CHN03 model (1000 particles)

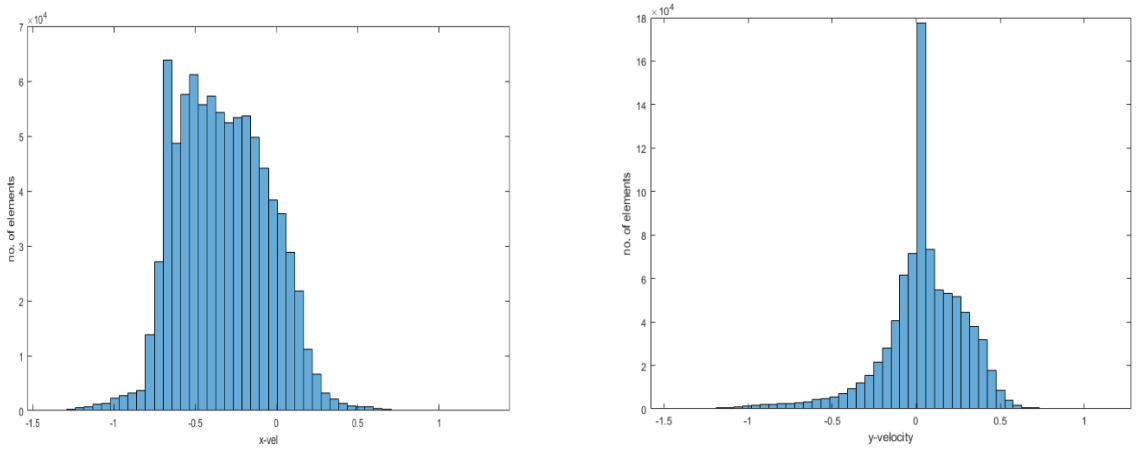

a) b)

Figure 34. PDF distribution of particles a) x-velocity; b) y-velocity

5.4.3 Numerical simulations for CT14 model

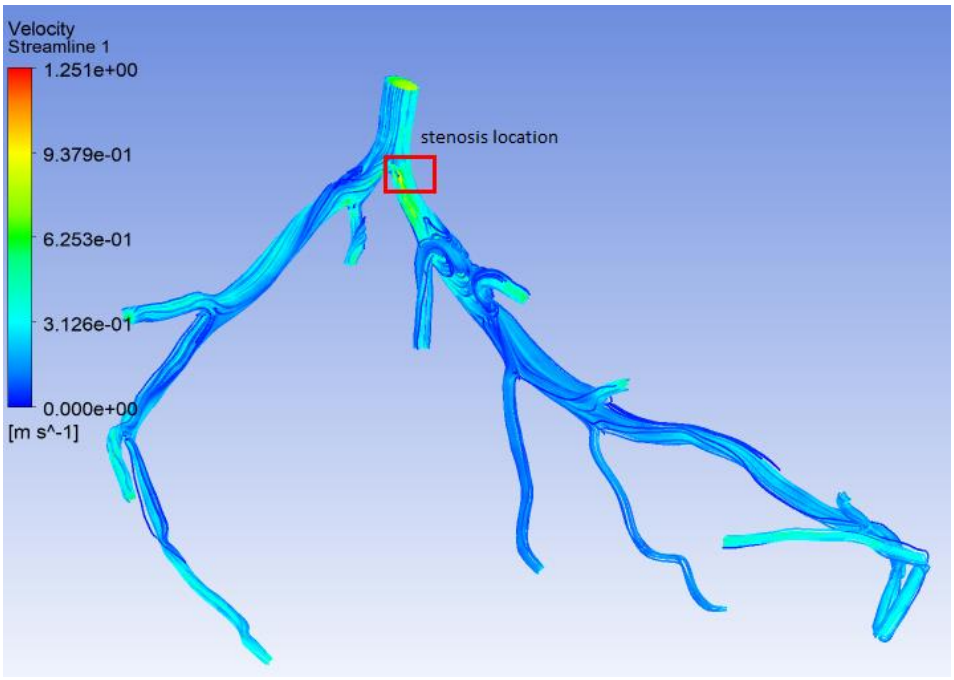

Figure 35. Velocity streamline for CT14 model

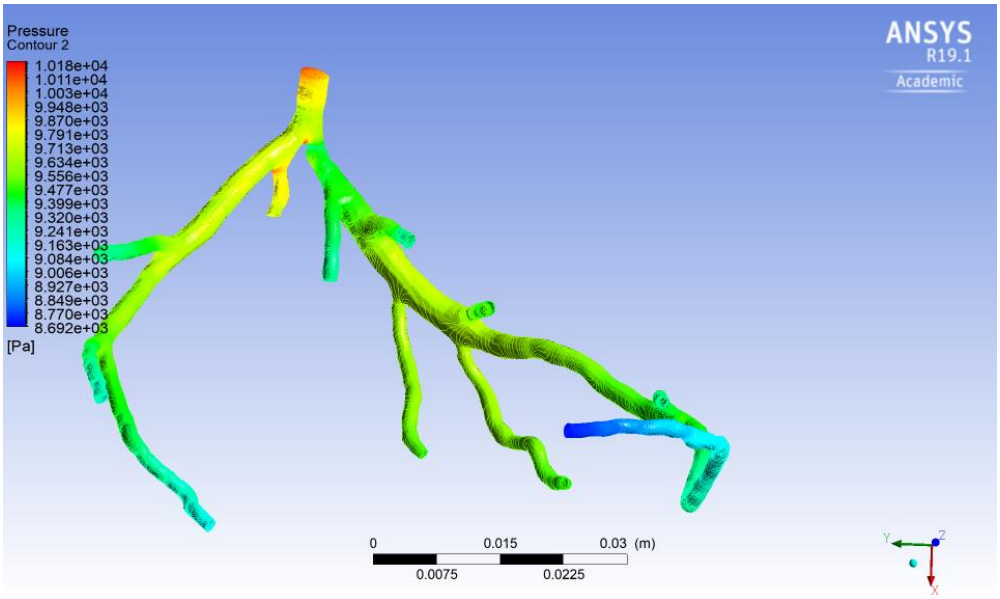

Figure 36. Pressure contour for CT14 model

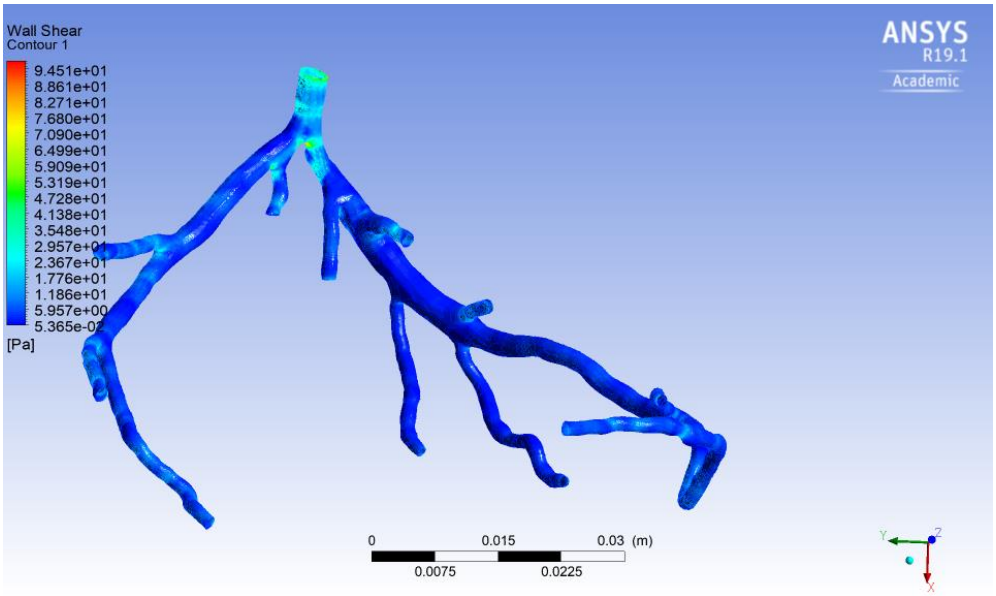

Figure 37. Wall Shear contour for CT14 model

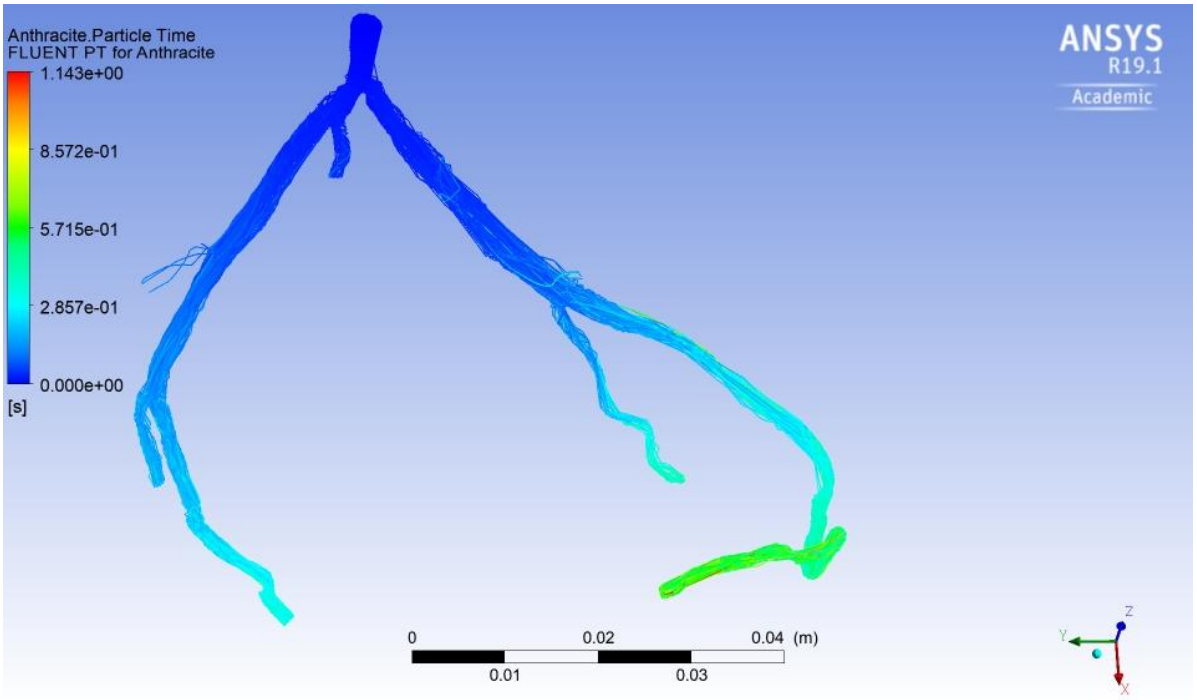

Figure 38. Particle time CT14 model

5.4.4 Numerical simulations for CT209 model

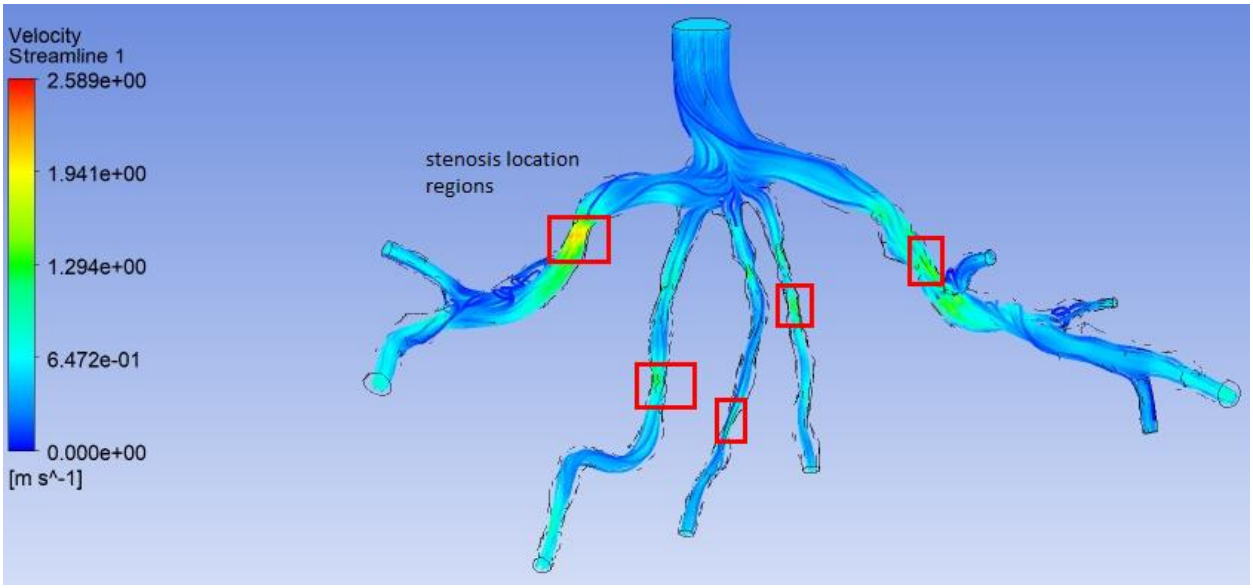

Figure 39. Velocity streamlines for CT209 model

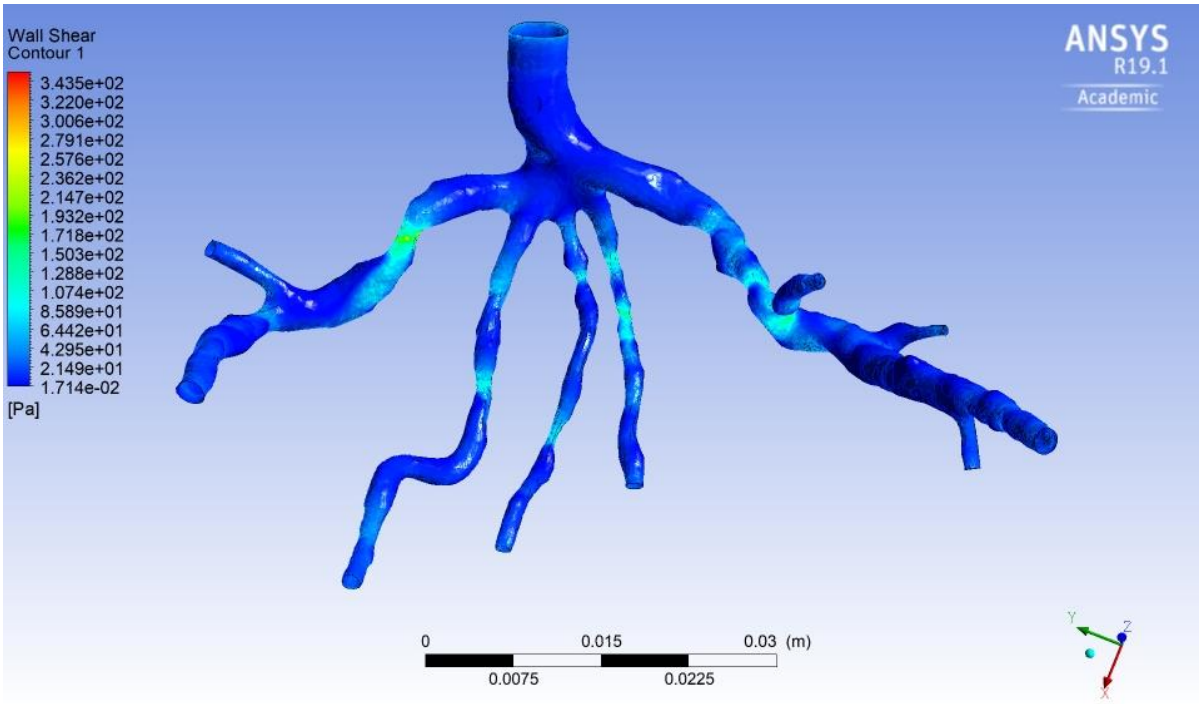

Figure 40. Wall Shear for CT209 model

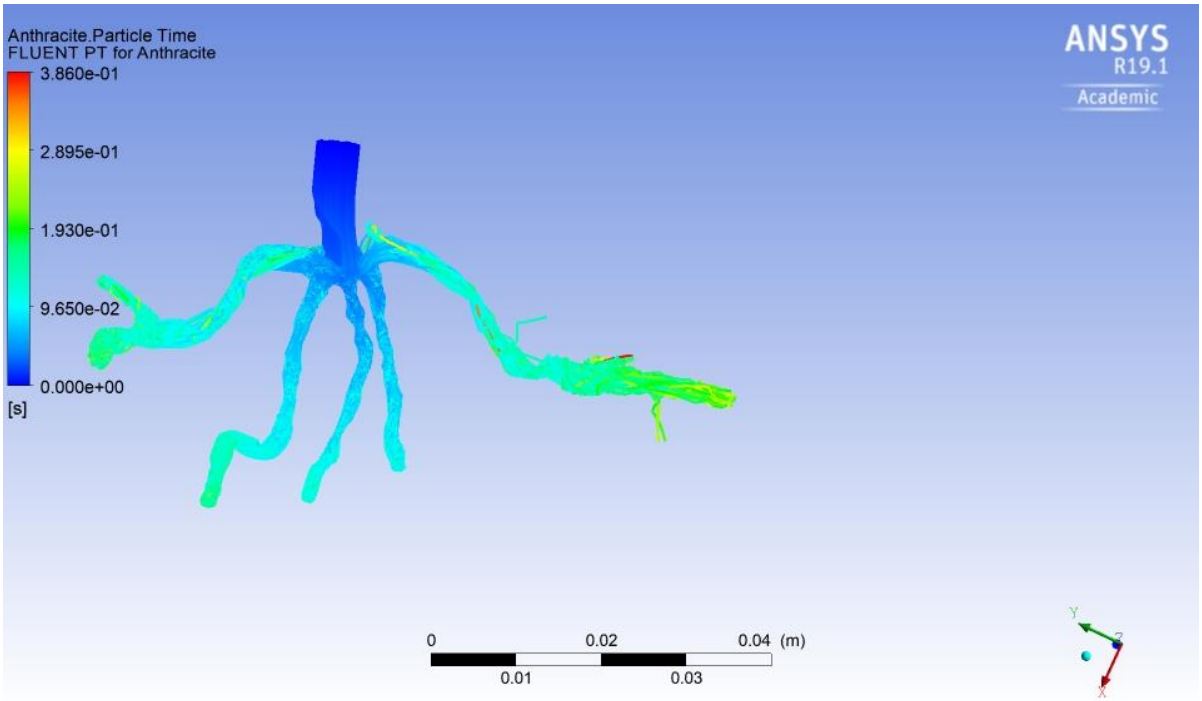

Figure 41. Particle time for CT209 model

5.4.5 Numerical simulations for CHN13 model

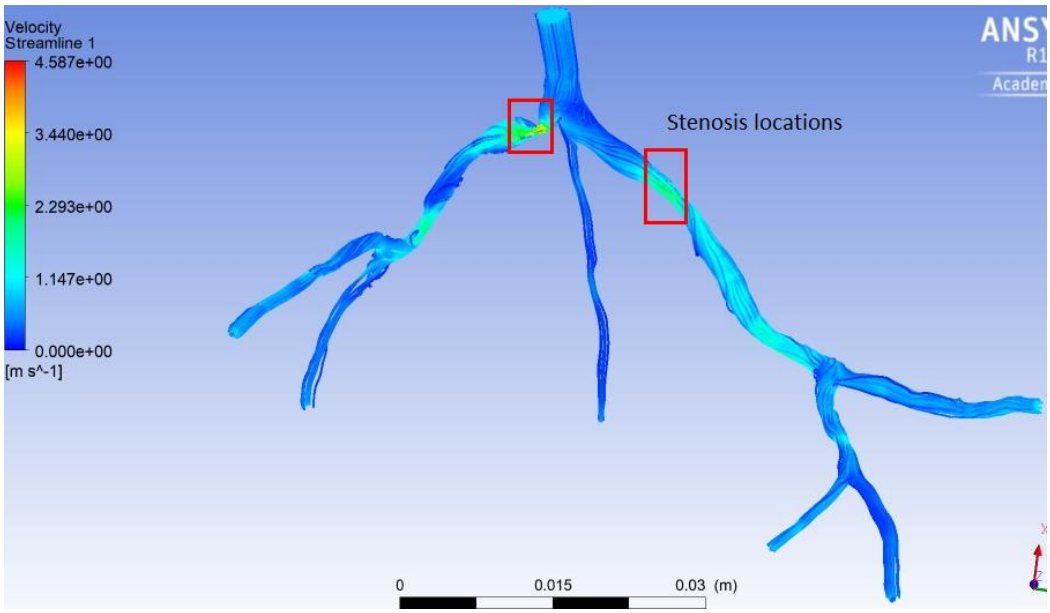

Figure 42. Velocity streamlines for CHN 13 model

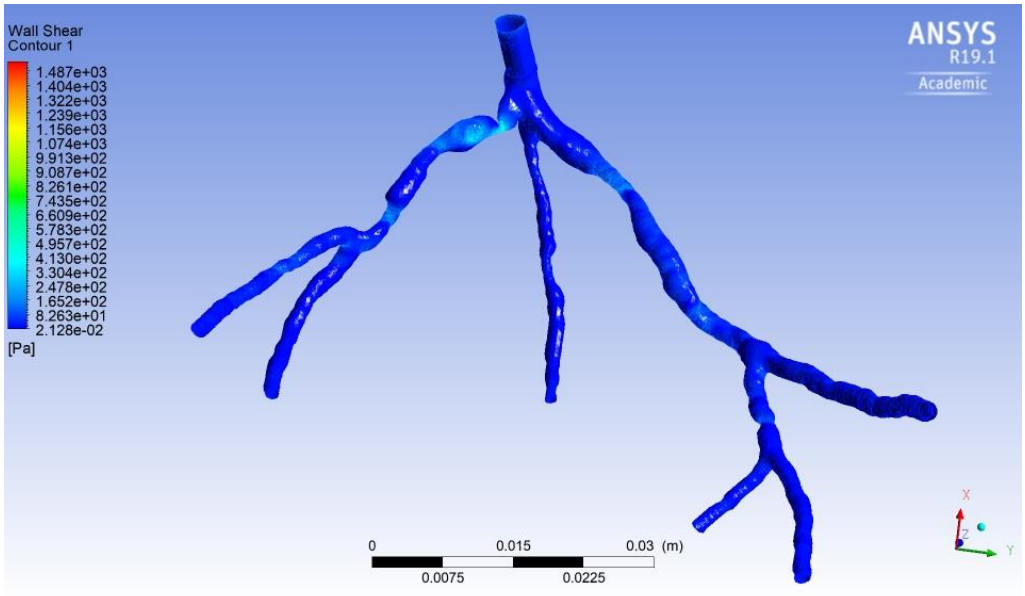

Figure 43. Wall Shear for CHN 13 model

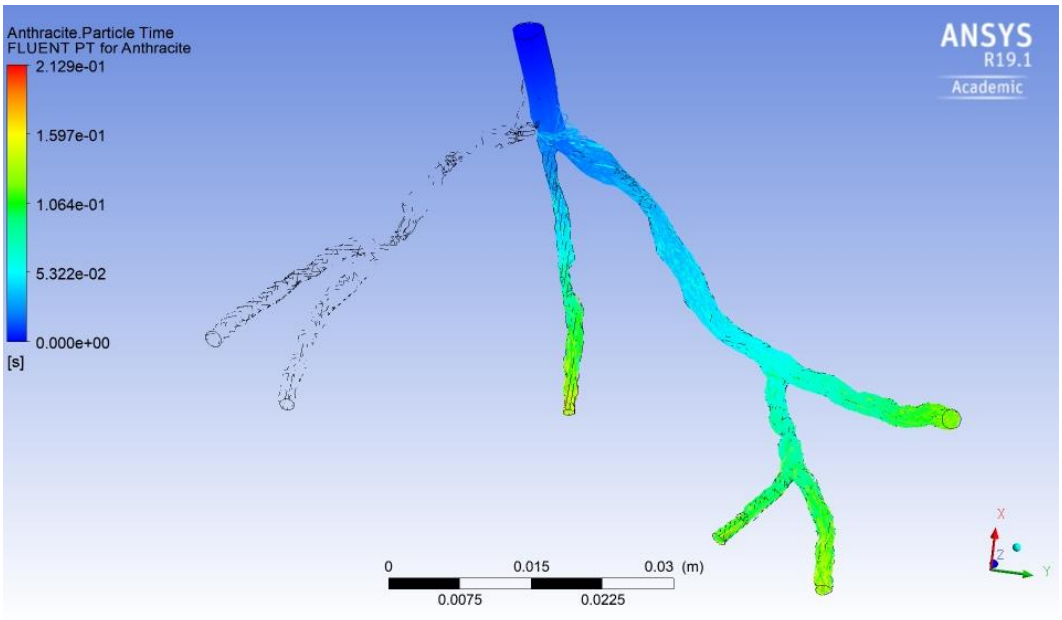

Figure 44. Particle time for CHN13 model

The numerical simulations have been performed in Ansys Fluent finite-element solver. For each model, the results have been post processed in Ansys CFD Post. The results that have been obtained for the four artery models, i.e. CHN03, CT14, CT209 and CHN13, are velocity streamlines, particle time, pressure contours and wall shear stress. Figures 24-27 illustrate simulation results for CHN03 artery model with 100 particles injected at the inlet. The velocity streamlines results for all artery models indicate the local velocity values at the particular regions of the branches. The locations where the artery cross-section narrows corresponds to the maximum values of velocity. Under the steady flow regime of blood, the decrease in area of the vessel wall implies higher velocity rate. That is true by continuity equation. In addition, the narrowed artery wall corresponds to the region of plaque accumulation, i.e. stenosis formation. Consequently, the stenotic region is formed at the branches, where the velocity flow is maximum. In Figure 24, the maximum velocity of 2.27 m/s is observed in the leftmost daughter branch. The red square boxes indicate the region of stenosis formation. The particle time results indicate the total time required for the particle to reach the distinct region of outlet branches. In the case of CHN03 model, the maximum particle time (0.387 s) is observed for the longest branch, located at the rightmost side. The pressure contour plots enable to estimate static pressure values within artery as well as pressure drop across the branch. For the all models considered, the wall shear stress reaches highest values at the stenotic regions. The particle track data contained information about the particles position and velocity components in three spatial coordinates (x, y, z) at each residence time value. The PDF distributions of particles' three velocity components have been plotted in MATLAB software against number of bin elements, represented by heights of individual rectangles that are equally distributed along horizontal axes. The number of bins corresponds to the total number of rectangles. The PDF distribution graphs of the particle velocities follow Gaussian distribution (Fig. 28). That implies that velocities of particles have settled within statistical convergence. Fig. 29 depicts histogram of velocity distributions of the single flow against number of bin counts.

5.5 Experimental results

Image intensity analysis of smoke

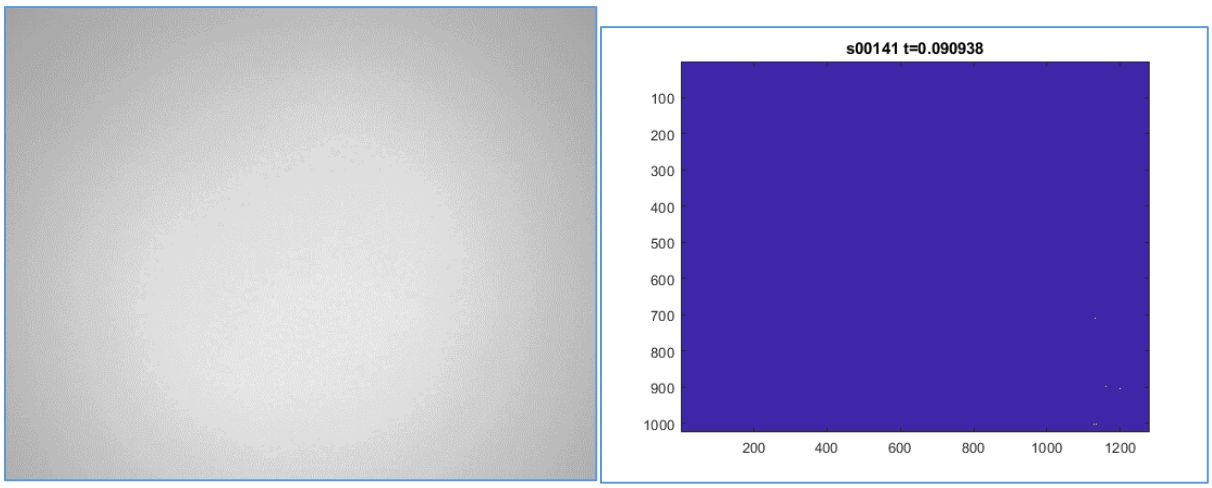

Figure 45. Camera Frame s00141 (Left) intensity 0 (Right)

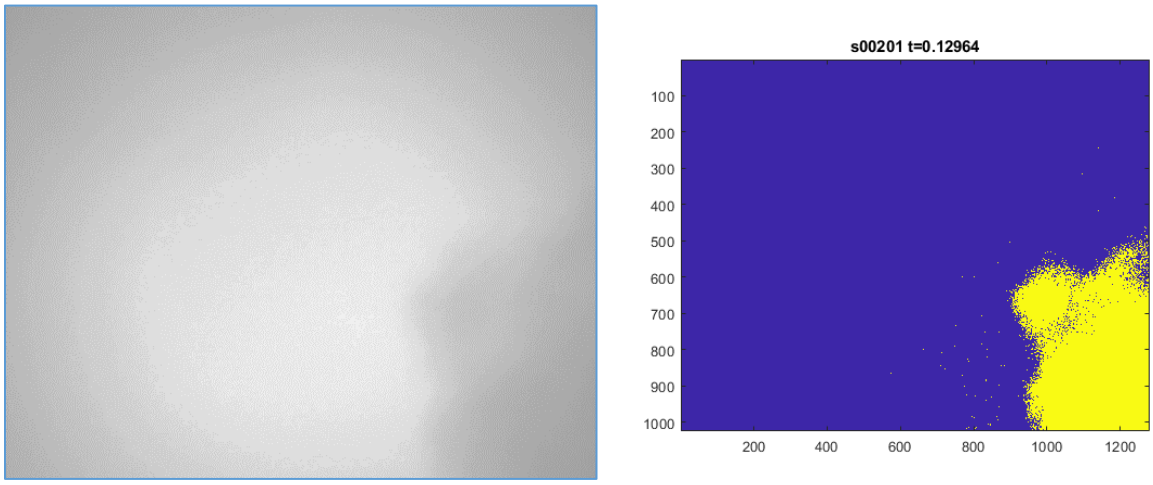

Figure 46. Camera Frame 00201 (Left) and intensity difference compared to reference frame (Right)

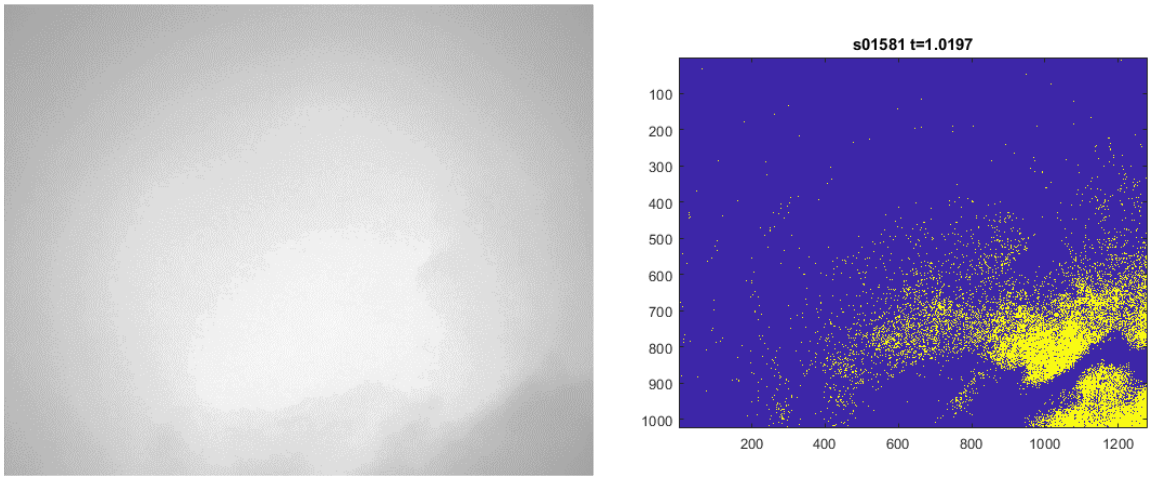

Figure 47 (a left) Camera Frame 1581 (b left) intensity difference compared to reference frame

Figure 45, 46 and 47 illustrates the actual frame from camera and MATLAB intensity analysis results. Smoke traveling region in 2D plane was detected per each frame. Comparison can be made with visual frame on the left and analyzed frame on the right. However, noises are present in results of intensity difference frames. In addition, effect of light source is sensible in intensity graphs.

Movement of smoke could be tracked with this preliminary code. However, it is not possible to measure the velocity of the flow and smoke cloud sizes cannot be detected from frames. Therefore, it is suggested to perform experiment with water droplet injection.

6. Conclusion

In the first part of the capstone project, LES and DNS methods have been implemented to generate statistically stationary HIT field. In order to achieve statistically stationary HIT, stochastic forcing term developed has been successfully added to the OpenFOAM solvers. Series of simulations were performed with different mesh sizes to study the effect of meshing to volume averaged velocity fluctuations. Grid size of N=256 have shown best performance when flow parameters of the simulations were analyzed. It was expected since small scales fully resolved at finer mesh sizes. Effect forcing time constant α on U' has been studied. The condition $t_f < t_\eta$ when energy dissipation rate remains constant (not decaying turbulence) has been achieved at simulation time of t=65s for N=256. In addition, fluctuations of large-scales values over time were increasing due to decrease of U'. However, slope of U' decrease tends to zero resulting in not decaying flow. The results obtained from DNS simulations showed that an increase of number of mesh elements led to smaller velocity fluctuations due to the better resolution of smaller scales.

Statistically stationary HIT could not be fully achieved for all variation of α in this work due to expensive computational time. Nevertheless, it was found that it is possible to control energy production region and U' magnitude with acceleration variance σ. Energy spectrum curve for scales present in HIT was obtained for N=256. Slope of energy spectrum follow suggested slope of $1.62k^{-5/4}$. Parallel computing approach with 8 cores (instead of single core) was developed for DNS solver that showed identical results for U' magnitude. Code development of parallel solution will be considered in future work to increase computational efficiency of simulations.

The simulations of particle phase were performed in Matlab and CFDEM. The results obtained from Matlab revealed several constraints of the solver. The interpolation of the velocity field was incorrect for the particles which left the flow domain. Additionally, in the simulations, the particles were presented as points rather than spheres. This made the physical model unrealistic. Finally, the simulations in Matlab were computationally expensive. The computational expensiveness was not a problem for a small number of mesh elements, however, for the simulations of N=256, it would be significantly. Then the simulations were performed in CFDEM software. Since the solver does not include forcing terms, the HIT was not reached. The decaying turbulence with particle phase was simulated. However, in order to investigate the dynamics of the particles, the HIT should be used for the flow phase. There are two possible solutions to this issue: write the libraries containing DNS solver and forcing term or change the solver in CFDEM to make it take the results from OpenFOAM simulations. It was decided to choose the second alternative since the results for flow simulations from OpenFOAM were already obtained. The new simulations of the flow domain will take a considerable amount of time.

The change of mean square separation with time was investigated and was represented on graphs with normalized scales. Firstly, it was concluded, that the higher velocity of the wind

corresponds to greater value of normalized initial separation between particles. Also, it was pointed out that the graphs for the different cases possess same features. On each graph two different parts were distinguished. The first part of graph is characterized by insignificant change of normalized mean square dispersion with time until the first decade, whereas the second part contains a lot of fluctuations. The fluctuations were caused by the limitations in tracking of the particles, which traveled long distances or traveled out from the tracking range. The scarcity of the long tracks leads to the fact that statistical convergence of results is not achieved on the second part of the graphs. To increase the long tracks' number it is required to apply cameras with higher acquisition rate during experiment. This allows to track the movement of each particle more accurately. Another method to avoid the shortage of long tracks is to use numerical simulations instead of experimental approach. As each inertial particle is tracked individually by computer thoughout simulation, the coordinates of all inertial particles are recorded on each time step. As a result, unlike experimental approach, all data regarding the coordinates of the particles is recorded throughout the simulation.

The applied studies involved numerical investigation of two-phase laminar flows in human coronary arteries via *Ansys Fluent* finite-element solver. The results of velocity streamlines, wall shear stress, pressure contour and particle time were obtained for the four models of coronary arteries. The dynamics of particles motion and their tracks have been obtained by implementation of Discrete Phase Model in the solver. The results of simulations, i.e. velocity contours, enabled to identify the regions of possible stenosis locations. In addition, it was observed that depending on the vessel geometry, number of daughter branches and diameter sizes, each artery have different number of stenotic regions and their locations. The PDF distributions of particle and flow velcoities has been plotted via MATLAB for CHN 03 model. The PDFs of particles velocities follow Gaussian distribution due to the significant number of statistics. However, the main flow distributions have not experienced Gaussian profile. The future works could involve implementing particle phase in an unsteady mode and injecting larger number of inertial particles at the inlet.

7. Reference list

[1]J. Bec, L. Biferale, M. Cencini, A. Lanotte, S. Musacchio and F. Toschi, "Heavy Particle Concentration in Turbulence at Dissipative and Inertial Scales", *Physical Review Letters*, vol. 98, no. 8, 2007. Available: 10.1103/physrevlett.98.084502 [Accessed 24 November 2019].

[2] L. Smoot, *Pulverized-coal Combustion and Gasification*. Springer Verlag, 2013.

[3]H. Zhou, G. Flamant and D. Gauthier, "DEM-LES of coal combustion in a bubbling fluidized bed. Part I: gas-particle turbulent flow structure", *Chemical Engineering Science*, vol. 59, no. 20, pp. 4193-4203, 2004. Available: 10.1016/j.ces.2004.01.069 [Accessed 24 November 2019].

[4]N. Qureshi, U. Arrieta, C. Baudet, A. Cartellier, Y. Gagne and M. Bourgoin, "Acceleration statistics of inertial particles in turbulent flow", *The European Physical Journal B*, vol. 66, no. 4, pp. 531-536, 2008. Available: 10.1140/epjb/e2008-00460-x [Accessed 24 November 2019].

[5] Kolmogorov, A. N. “The local structure of turbulence in incompressible viscous fluid for very large Reynolds numbers”, *Cr Acad. Sci. URSS*, vol. 30,pp. 301-305, 1941.

[6] E. Saw, R. Shaw, S. Ayyalasomayajula, P. Chuang and Á. Gylfason, "Inertial Clustering of Particles in High-Reynolds-Number Turbulence", *Physical Review Letters*, vol. 100, no. 21, 2008. Available: 10.1103/physrevlett.100.214501 [Accessed 24 November 2019].

[7] L. Wang and M. Maxey, "Settling velocity and concentration distribution of heavy particles in homogeneous isotropic turbulence", *Journal of Fluid Mechanics*, vol. 256, pp. 27-68, 1993. Available: 10.1017/s0022112093002708 [Accessed 24 November 2019].

[8] V. Michelassi, J. Wissink and W. Rodi, “Analysis of DNS and LES of flow in a low pressure turbine cascade with incoming wakes and comparison with experiments”, *Flow, Turbulence and Combustion*, vol. 69, no. 34, pp. 295-329, 2002. Available: 10.1023/a:1027334303200 [Accessed 24 November 2019].

[9] B. Rosa, H. Parishani, O. Ayala and L. Wang, "Settling velocity of small inertial particles in homogeneous isotropic turbulence from high-resolution DNS", *International Journal of Multiphase Flow*, vol. 83, pp. 217-231, 2016. Available: 10.1016/j.ijmultiphaseflow.2016.04.005 [Accessed 24 November 2019].

[10]R. Mei, "Effect of turbulence on the particle settling velocity in the nonlinear drag range", *International Journal of Multiphase Flow*, vol. 20, no. 2, pp. 273-284, 1994. Available: 10.1016/0301-9322(94)90082-5 [Accessed 24 November 2019].

[11] J. Stout, S. Arya and E. Genikhovich, "The Effect of Nonlinear Drag on the Motion and Settling Velocity of Heavy Particles", *Journal of the Atmospheric Sciences*, vol. 52, no. 22, pp. 3836-3848, 1995. Available: 10.1175/1520-0469(1995)052<3836:teondo>2.0.co;2 [Accessed 24 November 2019].

[12] P. Nielsen, "Turbulence Effects on the Settling of Suspended Particles", *SEPM Journal of Sedimentary Research*, vol. 63, 1993. Available: 10.1306/d4267c1c-2b26-11d7-8648000102c1865d [Accessed 24 November 2019].

[13]J. Fung, "Residence time of inertial particles in a vortex", *Journal of Geophysical Research: Oceans*, vol. 105, no. 6, pp. 14261-14272, 2000. Available: 10.1029/2000jc000260 [Accessed 24 November 2019].

[14]R. Vilela and A. Motter, "Can Aerosols Be Trapped in Open Flows?", *Physical Review Letters*, vol. 99, no. 26, 2007. Available: 10.1103/physrevlett.99.264101 [Accessed 24 November 2019].

[15] Good, P. Ireland, G. Bewley, E. Bodenschatz, L. Collins and Z. Warhaft, "Settling regimes of inertial particles in isotropic turbulence", *Journal of Fluid Mechanics*, vol. 759, 2014. Available: 10.1017/jfm.2014.602 [Accessed 24 November 2019].

[16]M. Maxey, "Equation of motion for a small rigid sphere in a nonuniform flow", *Physics of Fluids*, vol. 26, no. 4, p. 883, 1983. Available: 10.1063/1.864230 [Accessed 24 November 2019].

[19] M. El Rafei, L. Könözsy and Z. Rana, "Investigation of Numerical Dissipation in Classical and Implicit Large Eddy Simulations", *Aerospace*, vol. 4, no. 4, p. 59, 2017. Available: 10.3390/aerospace4040059 [Accessed 24 November 2019].

[20] B. Rosa, H. Parishani, O. Ayala and L. Wang, "Effects of forcing time scale on the simulated turbulent flows and turbulent collision statistics of inertial particles", *Physics of Fluids*, vol. 27, no. 1, p. 015105, 2015. Available: 10.1063/1.4906334 [Accessed 24 November 2019].

[21] V. Eswaran and S. Pope, "An examination of forcing in direct numerical simulations of turbulence", *Computers & Fluids*, vol. 16, no. 3, pp. 257-278, 1988. Available: 10.1016/0045-7930(88)90013-8 [Accessed 24 November 2019].
[22] N. Wax, Selected Papers on Noise and Stochastic Processes. Doer, New Yorl (1954).
[23] O. Ayala and L. Wang, "Parallel implementation and scalability analysis of 3D Fast Fourier Transform using 2D domain decomposition", *Parallel Computing*, vol. 39, no. 1, pp. 58-77, 2013. Available: 10.1016/j.parco.2012.12.002 [Accessed 24 November 2019].
[24] B. Rosa, H. Parishani, O. Ayala, W. Grabowski and L. Wang, "Kinematic and dynamic collision statistics of cloud droplets from high-resolution simulations", *New Journal of Physics*, vol. 15, no. 4, p. 045032, 2013. Available: 10.1088/1367-2630/15/4/045032 [Accessed 24 November 2019].
[25] O. Ayala, W. Grabowski and L. Wang, "A hybrid approach for simulating turbulent collisions of hydrodynamically-interacting particles", *Journal of Computational Physics*, vol. 225, no. 1, pp. 51-73, 2007. Available: 10.1016/j.jcp.2006.11.016 [Accessed 24 November 2019].
[26] C. Franklin, P. Vaillancourt and M. Yau, "Statistics and Parameterizations of the Effect of Turbulence on the Geometric Collision Kernel of Cloud Droplets", *Journal of the Atmospheric Sciences*, vol. 64, no. 3, pp. 938-954, 2007. Available: 10.1175/jas3872.1 [Accessed 24 November 2019].
[27] O. Ayala, H. Parishani, L. Chen, B. Rosa and L. Wang, "DNS of hydrodynamically interacting droplets in turbulent clouds: Parallel implementation and scalability analysis using 2D domain decomposition", *Computer Physics Communications*, vol. 185, no. 12, pp. 3269-3290, 2014. Available: 10.1016/j.cpc.2014.09.005 [Accessed 24 November 2019].
[28] O. Ayala, B. Rosa, L.-P. Wang, and W. W. Grabowski, "Effects of turbulence on the geometric collision rate of sedimenting droplets. Part 1. Results from direct numerical simulation," *New Journal of Physics*, vol. 10, no. 7, p. 075015, 2008.
[29] S. Elgobashi, "An Updated Classification Map of Particle-Laden Turbulent Flows", *Fluid Mechanics and Its Applications*, pp. 3-10. Available: 10.1007/1-4020-4977-3_1 [Accessed 24 November 2019].
[30] F. Greifzu, C. Kratzsch, T. Forgber, F. Lindner, and R. Schwarze, "Assessment of particle-tracking models for dispersed particle-laden flows implemented in OpenFOAM and ANSYS FLUENT," *Engineering Applications of Computational Fluid Mechanics*, vol. 10, no. 1, pp. 30–43, 2015.
[31] B. Vreman, B. J. Geurts, N. G. Deen, J. A. M. Kuipers, and J. G. M. Kuerten, "Two- and Four-Way Coupled Euler–Lagrangian Large-Eddy Simulation of Turbulent Particle-Laden Channel Flow," *Flow, Turbulence and Combustion*, vol. 82, no. 1, pp. 47–71, 2008.
[32] L. Wang, O. Ayala, Y. Xue and W. Grabowski, "Comments on "Droplets to Drops by Turbulent Coagulation"", *Journal of the Atmospheric Sciences*, vol. 63, no. 9, pp. 2397-2401, 2006. Available: 10.1175/jas3750.1.
[33] Lee, J. Y., & Lee, S. J. (2009). *Murray's law and the bifurcation angle in the arterial micro-circulation system and their application to the design of microfluidics. Microfluidics and Nanofluidics, 8(1), 85–95.* doi:10.1007/s10404-009-0454-1
[34] M. Bourgoin, "Turbulent pair dispersion as a ballistic cascade phenomenology," *Journal of Fluid Mechanics*, vol. 772, pp. 678–704, Aug. 2015.
[35] L. F. Richardson, "Atmospheric diffusion shown on a distance-neighbour graph," 1926.
[36] Batchelor and Obukov, "The application of the similarity theory of turbulence to atmospheric diffusion. ," *Quarterly Journal of the Royal Meteorological Society* , 1950.
[37] B. Sawford, "Turbulent Relative Dispersion," *Annual Review of Fluid Mechanics*, vol. 33, no. 1, pp. 289–317, 2001.
[38] J. P. Salazar and L. R. Collins, "Two-Particle Dispersion in Isotropic Turbulent Flows," *Annual Review of Fluid Mechanics*, vol. 41, no. 1, pp. 405–432, 2009.
[39] G. Boffetta and I. M. Sokolov, "Statistics of two-particle dispersion in two-dimensional turbulence," *Physics of Fluids*, vol. 14, no. 9, pp. 3224–3232, May 2002.
[40] L. Biferale, G. Boffetta, A. Celani, B. J. Devenish, A. Lanotte, and F. Toschi, "Lagrangian statistics of particle pairs in homogeneous isotropic turbulence," *Physics of Fluids*, vol. 17, no. 11, p. 115101, 2005.
[41] Zhao, Y., Sumbekova, S. et al. (2019). A New Physiologically Based Algorithm (PBA) for Outflow Boundary Conditions for CFD Estimation of Flow Fractional Reserve (FFR) in Coronary Artery Trees.

Nazarbayev University.
[42] Spaan, Jos A. "Physiological basis of clinically used coronary hemodynamic indices." *Circulation* 113.3 (2006): 446-455
[43] Mukherjee, D., Padilla, J. (2015). Numerical investigation of fluid-particle interactions for embolic stroke. Theoretical Comput. Fluid Dyn. Springer.
[44] Jung, J., Lyczkowski, R. et al. (2005). Multiphase hemodynamic simulation of pulsatile flow in coronary artery. Journal of Biomechanics 39: 2064-2073.
[45] Kaewbumrung, M., Orankitjaroen, S., Boonkrong, P., Nuntadilok, B., & Wiwatanapataphee, B. (2018). *Numerical Simulation of Dispersed Particle-Blood Flow in the Stenosed Coronary Arteries*. International Journal of Differential Equations, 1–16. doi:10.1155/2018/2593425
[46] Stelzenmuller, N., Polanco, J. I., Vignal, L., Vinkovic, I., & Mordant, N. (2017). Lagrangian acceleration statistics in a turbulent channel flow. *Physical Review Fluids*, *2*(5), 054602.
[47] S. Sumbekova, A. Cartellier, A. Aliseda, and M. Bourgoin, "Preferential concentration of inertial sub-Kolmogorov particles: The roles of mass loading of particles, Stokes numbers, and Reynolds numbers," *Physical Review Fluids*, vol. 2, no. 2, Aug. 2017.

Appendix

Brief	Numerical and Experimental Investigation of multiphase flows. Fundamental and Applied studies	This project is designed for a numerical and experimental investigation of multiphase (two phase) flows in fundamental fluid mechanics and applied biomechanics. The fundamental study and its numerical part consists of the studies of the turbulent flow laden with inertial particles: the flow phase will be resolved using Large-Eddy (LES) and Direct Navier Stokes (DNS) simulations, and particle phase will be resolved using Discrete Element Method. The applied study will consist of resolving the flow in human organs such as coronary arteries, adding the equation of motion for the inertial particles represented by the blood clots and dust particles, using the commercially available and open source software such as ANSYS and Simvascular. As part of the project, both fundamental and applied studies will include the investigation of the dynamics of particle laden flows. The pair dispersion of inertial particles in turbulent flow will be investigated for available experimental data. Two-phase flows validation will be performed in the second term using either the experimentally and numerically available data or gathered experimental data, prelimenary experiment set up to study of motion of smoke clouds in air.	Asset Zhamiyev, Nurzhan Maldenov, Bekbolat Adekenov and Arman Abylkassimov	96
WP1	Literature review of LES, DNS; numericqal simulations, experimental study	Literature review of large-eddy simulation (LES) and Direct navier stokes (DNS) simulations of turbulent flows setting up homogeneous isotropic turbulent with Taylor-Green Vortex initial condiiton, setting up numerical schemes and simulation parameters, discussion of simulation results, preliminary experiment with smoke, preliminary setting up of experimental procedures for fundamental studies	Asset Zhamiyev	6
WP2	Literature review of particle tracking techniques; numerical simulations of particle phase, DNS simulations, experimental study	Direct navier stokes (DNS) simulations of turbulent flows,Literature review on studies about clustering and settling of inertial particles in homogeneous isotropic turbulent flow, development of numerical scheme for particle tracking, analysis and discussion of the obtained results, preliminary experiment with smoke, preliminary setting up of experimental procedures for fundamental studies	Nurzhan Maldenov	6

WP3	Literature review of pair dispersion; calculation of pair dispersion of inertial particles; experimental study	Literature review of pair dispersion , pair dispersion of inertial particles in turbulent flow for available experimental data, discussion of the results, preliminary experiment with smoke, preliminary setting up of experimental procedures for fundamental studies	Bekbolat Adekenov	6
WP4	Numerical simulation of coronary arteries and laden with inertial particles using ANSYS and MATLAB ,experimental study	Literature review about coronary arteries , numerical data of flows in humans organs, i.e. coronary arteries would be performed via ANSYS and Matlab commercial software. The inertial particles motion would be analyzed via equations representing the motion of blood clot particles, preliminary experiment with smoke, preliminary setting up of experimental procedures for fundamental studies	Arman Abylkassimov	6

Particle Simulation code

```
m = 16;
n = 4096;
L = 2*pi;
deltaT = 0.005;
t0 = 40.000;
% Import of wolfram files in matlab (Vx, Vy, Vz)
k = 1;
for t=40:deltaT:40.04
i = (t-40)/deltaT;
% 'C:\\Users\\nurzhan.maldenov\\Desktop\\SAMPLES\\g%',t
f = sprintf('C:\\Users\\Малденов НУржан\\Desktop\\SAMPLE_10\\%g',t);
U_x = sprintf('Ux.');
U_y = sprintf('Uy.');
U_z = sprintf('Uz.');
time(1,k)=t;
Ux(1:n,(k)) = dlmread(fullfile(f,U_x),",[25 0 4120 0]);
Uy(1:n,(k)) = dlmread(fullfile(f,U_y),",[25 0 4120 0]);
Uz(1:n,(k)) = dlmread(fullfile(f,U_z),",[25 0 4120 0]);
k = k+1;
end
% Positions of particles
% Assessment of location
% range is within the range from 0 to pi/6
% Number of points is 512
Xp = 2.125:0.25:3.875;
Yp = 2.125:0.25:3.875;
Zp = 2.125:0.25:3.875;
```

```
i = 1;
j = 1;
k = 1;
N = 1;
for i = 1:1:8
x = 2.125+0.25*(i-1);
for j = 1:1:8
y = 2.125+0.25*(j-1);
for k = 1:1:8
z = 2.125+0.25*(k-1);
ZP(:,N) = x;
YP(:,N) = y;
XP(:,N) = z;
Pos(:,N) = [z;y;x];
N = N+1;
end
end
end
Pos(:,:,2) = zeros(3,512);
Pos(:,:,3) = zeros(3,512);
Pos(:,:,4) = zeros(3,512);
Pos(:,:,5) = zeros(3,512);
% Positions corresponding to velocity
for i = 1:1:16
Zf(i) = L/(2*m)+(L/m)*(i-1);
for j = 1:1:16
Yf(j) = L/(2*m)+(L/m)*(j-1);
for k = 1:1:16
Xf(k) = L/(2*m)+(L/m)*(k-1);
Num = k+(j-1)*16+(i-1)*256;
Loc(:,Num) = [Xf(k) Yf(j) Zf(i)];
end
end
end
% Interpolation of Velocity of particles
% Hermite polynomial
[X,Y,Z] = meshgrid(Xf,Yf,Zf)
Xq = XP;
Yq = YP;
Zq = ZP;
% [Xq,Yq,Zq] = meshgrid(Xp,Yp,Zp)
Ux_0 = Ux(:,1);
Uy_0 = Uy(:,1);
Uz_0 = Uz(:,1);
% converting velocity vectors in matrix form
j = 1;
k = 1;
V = zeros(3,512);
V(:,:,2) = zeros(3,512);
V(:,:,3) = zeros(3,512);
N = 1;
for i = 1:1:9
for o = 1:1:4096
k = fix((o-1)/256)+1;
```

```
j = fix((o-1-(k-1)*256)/16)+1;
if rem(o,16) == 0
l = 16;
else
l = rem(o,16);
end
U_xf(j,l,k) = Ux(o,i);
U_yf(j,l,k) = Uy(o,i);
U_zf(j,l,k) = Uz(o,i);
gh = 56
end
U_xq = interp3(X,Y,Z,U_xf,Xq,Yq,Zq,'cubic');
U_yq = interp3(X,Y,Z,U_yf,Xq,Yq,Zq,'cubic');
U_zq = interp3(X,Y,Z,U_zf,Xq,Yq,Zq,'cubic');

g_x = zeros(1,512);
g_y = ones(1,512)*(-9.801);
g_z = zeros(1,512);
g = [g_x;g_y;g_z];

U(:,:,i) = [U_xq; U_yq; U_zq]
% Maxey-Riley equation
% Tau_P
Tau_Ita = sqrt(1.7*(10)^(-5)/0.2);
St = 0.1;
Tau_P = St*Tau_Ita;
V(:,:,i+1) = V(:,:,i) - deltaT/Tau_P*(V(:,:,i) - U(:,:,i)) + g*deltaT;
Pos(:,:,i+1) = V(:,:,i)*deltaT + Pos(:,:,i);
Xq = Pos(1,:,i+1)
Yq = Pos(2,:,i+1)
Zq = Pos(3,:,i+1)
% [Xq,Yq,Zq] = meshgrid(Xq1,Yq1,Zq1)
end
% graphs
% Particles(:,:) = Pos(:,:,6);
% Check
Xc = [2.945 2.945 2.9466 2.9415 2.9657 2.8625 3.3167 1.2955 10.2089 -29.2446];
Yc = [2.945 2.945 2.9607 2.907 3.1605 2.0552 6.9599 -14.743 81.2273 -343.3018];
Zc = [2.945 2.945 2.9426 2.9509 2.9118 3.0822 2.3331 5.6469 -9.038 55.89];
%plot3(Pos(1,:,1),Pos(2,:,1),Pos(3,:,1),'.','MarkerSize',50)
% axis([0 2*pi 0 2*pi 0 2*pi])
```

Pair-dispersion code

Code, which draws the graphs

```
clearvars D2_average D2_normalised D2_raw t T

n=0.431;
tau=0.011;
 k=0;
 Numel=arrayfun(@(X)(numel(X.dRD2)),meanD2_general);
 Max=max(Numel);
for i=1:1:Max
    D2_sum=0;
     k=k+1;
     m=0;
```

```
   for j=1:1:62
       D2_raw=meanD2_general(j+1).dRD2;   % Don't Forget to change tau and ita
       if numel(D2_raw)>=k
       D2=abs(D2_raw(1,k));    %for abs(D2_raw(1,k))
       D2_sum=D2_sum+D2;
       m=m+1;
       end
   end
   D2_average(i,1)=D2_sum/m;
   t(i,1)=1/2600*(i-1);
end
T=t./tau;
D2_normalised=D2_average./n^2;
figure
loglog(T,D2_normalised);
```

Code, which calculates the average value of results, obtained from 20 different movies.

```
clearvars D2_average RD2_average  R2_average meanD2_general

   for e=2:1:63
       for i=1:20
           string_part =
'D:\Study\Research\Results\MeanD2\meanD2_0p3_0p8_2p5_tracks\meanD2_0p3_0p8_2p5_tracks_';

filename1 = [string_part int2str(i) '_50_100ita.mat'];
load(filename1);
A(i).dRD2=meanD2(e).dRD2;
A(i).dD2=meanD2(e).dD2;
A(i).dR2=meanD2(e).dR2;
       end
       Numel=arrayfun(@(X)(numel(X.dRD2)),A);
       Max=max(Numel);
       k=0;
for i=1:1:Max
    D2_sum=0;
     k=k+1;
     m=0;
   for j=1:1:20
       D2_raw=A(j).dD2;
       if numel(D2_raw)>=k
       D2=D2_raw(1,k);
       D2_sum=D2_sum+D2;
       m=m+1;
       end
   end
   D2_average(i,1)=D2_sum/m;
   %t(i,1)=1/2600*(i-1);
end
k=0;
for i=1:1:Max
    RD2_sum=0;
     k=k+1;
     m=0;
   for j=1:1:20
       RD2_raw=A(j).dRD2;
       if numel(RD2_raw)>=k
       RD2=RD2_raw(1,k);
       RD2_sum=RD2_sum+RD2;
       m=m+1;
       end
   end
   RD2_average(i,1)=RD2_sum/m;
   %t(i,1)=1/2600*(i-1);
end
k=0;
for i=1:1:Max
    R2_sum=0;
     k=k+1;
     m=0;
   for j=1:1:20
       R2_raw=A(j).dR2;
```

```
        if numel(R2_raw)>=k
        R2=R2_raw(1,k);
        R2_sum=R2_sum+R2;
        m=m+1;
        end
    end
    R2_average(i,1)=R2_sum/m;
    %t(i,1)=1/2600*(i-1);
end
meanD2_general(e).dRD2=(RD2_average)';
meanD2_general(e).dD2=(D2_average)';
meanD2_general(e).dR2=(R2_average)';
    end
```

Code, which sorts inertial particles in all possible combinations of pairs and calculates the mean square dispersion.

```
str1=["0p3_0p8_10_tracks";
      "0p3_1p2_2p5_tracks";
      "0p3_1p2_5_tracks";
      "0p3_1p2_7p5_tracks";
      "0p3_1p2_10_tracks";
      "0p4_1p9_2p5_tracks";
      "0p4_1p9_5_tracks";
      "0p4_1p9_7p5_tracks";
      "0p4_1p9_10_tracks";
      "0p4_1p43_5_tracks";
      "0p4_1p43_7p5_tracks";
      "0p4_1p43_10_tracks";
      "0p5_1p9_2p5_tracks";
      "0p5_1p9_5_tracks";
      "0p5_1p9_7p5_tracks";
      "0p5_1p9_10_tracks"];
 ita_array=[0.114,
       0.429,
       0.255,
       0.174,
       0.118,
       0.439,
       0.260,
       0.174,
       0.121,
       0.252,
       0.166,
       0.118,
       0.442,
       0.249,
       0.168,
       0.120];
for jj=1:16
    ita=ita_array(jj);
    str=string(str1(jj));
for i=1:20

    string_part = 'G:\Bekbolat Adekenov\Filtered Tracks\';  % string_part = 'G:\Bekbolat
Adekenov\Filtered Tracks\vtracks_0p3_0p8_5_tracks\vtracks_0p3_0p8_5_tracks_';

filename11 =[string_part 'vtracks_' str '\vtracks_' str '_' int2str(i) '.mat'];
filename1 =join(filename11,"");
load(filename1);

%load('E:\TRACKS\TRACKS\0p4_7p5\tracked_vel_voronoii_1.mat');
%vtracks_ = vtracks(1:5000,1); %vtracks_0p3_0p8_2p5_tracks_1_50
vtracks_1=vtracks_filtered;
%% rearrange data "per image" instead of "per track"
part=track2part(vtracks_1);


%% Compute pair distances for all images
```

```
Fech=2600;
for k=1:numel(part)
    NN=numel(part(k).X);
    X1=ones(NN,1)*part(k).X;
    X2=part(k).X'*ones(1,NN);
    %dX2=(X2-X1).^2;
    dX=reshape(triu((X2-X1)),1,[]);    %

    Y1=ones(NN,1)*part(k).Y;
    Y2=part(k).Y'*ones(1,NN);
    %dY2=(Y2-Y1).^2;
    dY=reshape(triu((Y2-Y1)),1,[]);

    dR2=(dX.^2+dY.^2);

    dNtrack1=ones(NN,1)*part(k).Ntrack;
    dNtrack2=part(k).Ntrack'*ones(1,NN);
    %dNtrack=dNtrack2+i*dNtrack1;
    dNtrack=reshape(triu(dNtrack2+i*dNtrack1),1,[]);  %???

    %II=find(dD2==0);
    %dX2(II)=[];
    %dY2(II)=[];
    %dD2(II)=[];
    %dNtrack(II)=[];

    part(k).dX=dX;
    part(k).dY=dY;
    part(k).dR2=dR2;
    part(k).dNtrack=dNtrack;

    clear dX2 dY2 dD2 dNtrack II NN;
end

%% part2track for pairs
dNtrack=[part.dNtrack];
dNtrackU=unique(dNtrack);
dX=[part.dX];
dY=[part.dY];
dR2=[part.dR2];

dNtrackL=gpuArray(dNtrack);
dNtrackUS=gpuArray(dNtrackU);
dX=gpuArray(dX);
dY=gpuArray(dY);
dR2=gpuArray(dR2);



for k=1:numel(dNtrackUS)
   II=find(dNtrackL==dNtrackUS(k));
   trackpairGpu(k).dX=dX(II);
   trackpairGpu(k).dY=dY(II);
   trackpairGpu(k).dR2=dR2(II);
   trackpairGpu(k).dNtrack=dNtrackUS(k);
end

for k=1:numel(dNtrackUS)
 trackpair(k).dX=gather(trackpairGpu(k).dX);
   trackpair(k).dY=gather(trackpairGpu(k).dY);
   trackpair(k).dR2=gather(trackpairGpu(k).dR2);
   trackpair(k).dNtrack=gather(trackpairGpu(k).dNtrack);
end



%% define initial separations and binnings
Nbins=64;
%Dmax=3.828; %you have to set this value to be the maximum separation you want to explore, now it
is set for 100mm (assuming your data is in mm)
```

```
Dmax=100*ita;

dX0=arrayfun(@(X)(abs(X.dX(1))),trackpair);
dY0=arrayfun(@(X)(abs(X.dY(1))),trackpair);
dR20=arrayfun(@(X)(X.dR2(1)),trackpair);

edgesX=linspace(0,Dmax,Nbins);
edgesY=linspace(0,Dmax,Nbins);
edgesR2=linspace(0,Dmax^2,Nbins);

binX=(edgesX(2:end)+edgesX(1:end-1))/2;
binY=(edgesY(2:end)+edgesY(1:end-1))/2;
binR2=(edgesR2(2:end)+edgesR2(1:end-1))/2;

%%
[NX,binX0]=histc(dX0,edgesX);
[NY,binY0]=histc(dY0,edgesY);
[NR2,binR20]=histc(dR20,edgesR2);

for k=2:numel(binX)
 %   IX=find(binX0==k);
%    IY=find(binY0==k);
    IR=find(binR20==k);
% for statistics on 1D separation, we still condition on the 2D separation
% R20 to avoid combining for instance particles with small separation in X but actually very much
separated in Y
    IX=IR;
    IY=IR;
    dX2=arrayfun(@(X)((X.dX-X.dX(1)).^2),trackpair(IX),'UniformOutput',false);
    dY2=arrayfun(@(X)((X.dY-X.dY(1)).^2),trackpair(IY),'UniformOutput',false);
    dR2=arrayfun(@(X)(X.dR2-X.dR2(1)),trackpair(IR),'UniformOutput',false);
    dD2=arrayfun(@(X)((X.dX-X.dX(1)).^2+(X.dY-X.dY(1)).^2),trackpair(IR),'UniformOutput',false);
    dRD2=arrayfun(@(X)(X.dR2),trackpair(IR),'UniformOutput',false);

    NX=cellfun(@(X)(numel(X)),dX2);
    NY=cellfun(@(X)(numel(X)),dY2);
    NR=cellfun(@(X)(numel(X)),dR2);
    ND=cellfun(@(X)(numel(X)),dD2);
    NRD=cellfun(@(X)(numel(X)),dRD2);

    MX2=NaN(numel(dX2),max(NX));
    MY2=NaN(numel(dY2),max(NY));
    MR2=NaN(numel(dD2),max(NR));
    MD2=NaN(numel(dD2),max(ND));
    MRD2=NaN(numel(dRD2),max(NRD));

    for kk=1:numel(dX2)
        MX2(kk,1:NX(kk))=dX2{kk};
    end

    for kk=1:numel(dY2)
        MY2(kk,1:NY(kk))=dY2{kk};
    end

    for kk=1:numel(dR2)
        MR2(kk,1:NR(kk))=dR2{kk};
    end

    for kk=1:numel(dD2)
        MD2(kk,1:ND(kk))=dD2{kk};
    end

    for kk=1:numel(dRD2)
        MRD2(kk,1:NRD(kk))=dRD2{kk};
    end

    dX2=nanmean(MX2,1);
    dY2=nanmean(MY2,1);
    dR2=nanmean(MY2,1);
    dD2=nanmean(MD2,1);
    dRD2=nanmean(MRD2,1);
```

```
    dX2(dX2==NaN)=[];
    dY2(dY2==NaN)=[];
    dR2(dR2==NaN)=[];
    dD2(dD2==NaN)=[];
    dRD2(dRD2==NaN)=[];

    meanD2(k).dX2=nanmean(MX2,1);
    meanD2(k).dY2=nanmean(MY2,1);
    meanD2(k).dR2=nanmean(MR2,1);
    meanD2(k).dD2=nanmean(MD2,1);
     meanD2(k).dRD2=nanmean(MRD2,1);
    meanD2(k).TX=[0:numel(dX2)-1]/Fech;% you need to define Fech (sampling frequencey) in the
workspace
    meanD2(k).TY=[0:numel(dY2)-1]/Fech;% you need to define Fech (sampling frequencey) in the
workspace
    meanD2(k).TR=[0:numel(dR2)-1]/Fech;% you need to define Fech (sampling frequencey) in the
workspace
    meanD2(k).TD=[0:numel(dD2)-1]/Fech;% you need to define Fech (sampling frequencey) in the
workspace
    meanD2(k).dX20=mean(arrayfun(@(X)(X.dX(1).^2),trackpair(IR)));
    meanD2(k).dY20=mean(arrayfun(@(X)(X.dY(1).^2),trackpair(IR)));
    meanD2(k).dR20=binR2(k);
     clear MX2;
end

string_part_2 = 'G:\Bekbolat Adekenov\Results\results_';   %string_part_2 = 'G:\Bekbolat
Adekenov\Results\results_0p3_0p8_5_tracks\meanD2_0p3_0p8_5_tracks\meanD2_0p3_0p8_5_tracks_';
filename22 = [string_part_2 str '\meanD2_' str '\meanD2_' str '_' int2str(i) '_100ita.mat'];
filename2 =join(filename22,"");
save(filename2,'meanD2')

string_part_3 = 'G:\Bekbolat Adekenov\Results\results_';    %string_part_3 = 'G:\Bekbolat
Adekenov\Results\results_0p3_0p8_5_tracks\trackpair_0p3_0p8_5_tracks\trackpair_0p3_0p8_5_tracks_'
;
filename33 = [string_part_3 str '\trackpair_' str '\trackpair_' str '_' int2str(i) '.mat'];
filename3 =join(filename33,"");
save(filename3,'trackpair')


clearvars MX2 MY2 MR2 MD2 MRD2


Nbins=64;
%Dmax=3.828; %you have to set this value to be the maximum separation you want to explore, now it
is set for 100mm (assuming your data is in mm)
Dmax=60*ita;

dX0=arrayfun(@(X)(abs(X.dX(1))),trackpair);
dY0=arrayfun(@(X)(abs(X.dY(1))),trackpair);
dR20=arrayfun(@(X)(X.dR2(1)),trackpair);

edgesX=linspace(0,Dmax,Nbins);
edgesY=linspace(0,Dmax,Nbins);
edgesR2=linspace(0,Dmax^2,Nbins);

binX=(edgesX(2:end)+edgesX(1:end-1))/2;
binY=(edgesY(2:end)+edgesY(1:end-1))/2;
binR2=(edgesR2(2:end)+edgesR2(1:end-1))/2;

%%
[NX,binX0]=histc(dX0,edgesX);
[NY,binY0]=histc(dY0,edgesY);
[NR2,binR20]=histc(dR20,edgesR2);

for k=2:numel(binX)
 %   IX=find(binX0==k);
%    IY=find(binY0==k);
    IR=find(binR20==k);
% for statistics on 1D separation, we still condition on the 2D separation
```

```
% R20 to avoid combining for instance particles with small separation in X but actually very much
separated in Y
    IX=IR;
    IY=IR;
    dX2=arrayfun(@(X)((X.dX-X.dX(1)).^2),trackpair(IX),'UniformOutput',false);
    dY2=arrayfun(@(X)((X.dY-X.dY(1)).^2),trackpair(IY),'UniformOutput',false);
    dR2=arrayfun(@(X)(X.dR2-X.dR2(1)),trackpair(IR),'UniformOutput',false);
    dD2=arrayfun(@(X)((X.dX-X.dX(1)).^2+(X.dY-X.dY(1)).^2),trackpair(IR),'UniformOutput',false);
    dRD2=arrayfun(@(X)(X.dR2),trackpair(IR),'UniformOutput',false);

    NX=cellfun(@(X)(numel(X)),dX2);
    NY=cellfun(@(X)(numel(X)),dY2);
    NR=cellfun(@(X)(numel(X)),dR2);
    ND=cellfun(@(X)(numel(X)),dD2);
    NRD=cellfun(@(X)(numel(X)),dRD2);

    MX2=NaN(numel(dX2),max(NX));
    MY2=NaN(numel(dY2),max(NY));
    MR2=NaN(numel(dD2),max(NR));
    MD2=NaN(numel(dD2),max(ND));
    MRD2=NaN(numel(dRD2),max(NRD));

    for kk=1:numel(dX2)
        MX2(kk,1:NX(kk))=dX2{kk};
    end

    for kk=1:numel(dY2)
        MY2(kk,1:NY(kk))=dY2{kk};
    end

    for kk=1:numel(dR2)
        MR2(kk,1:NR(kk))=dR2{kk};
    end

    for kk=1:numel(dD2)
        MD2(kk,1:ND(kk))=dD2{kk};
    end

    for kk=1:numel(dRD2)
        MRD2(kk,1:NRD(kk))=dRD2{kk};
    end

    dX2=nanmean(MX2,1);
    dY2=nanmean(MY2,1);
    dR2=nanmean(MY2,1);
    dD2=nanmean(MD2,1);
    dRD2=nanmean(MRD2,1);

    dX2(dX2==NaN)=[];
    dY2(dY2==NaN)=[];
    dR2(dR2==NaN)=[];
    dD2(dD2==NaN)=[];
    dRD2(dRD2==NaN)=[];

    meanD2(k).dX2=nanmean(MX2,1);
    meanD2(k).dY2=nanmean(MY2,1);
    meanD2(k).dR2=nanmean(MR2,1);
    meanD2(k).dD2=nanmean(MD2,1);
     meanD2(k).dRD2=nanmean(MRD2,1);
    meanD2(k).TX=[0:numel(dX2)-1]/Fech;% you need to define Fech (sampling frequencey) in the
workspace
    meanD2(k).TY=[0:numel(dY2)-1]/Fech;% you need to define Fech (sampling frequencey) in the
workspace
    meanD2(k).TR=[0:numel(dR2)-1]/Fech;% you need to define Fech (sampling frequencey) in the
workspace
    meanD2(k).TD=[0:numel(dD2)-1]/Fech;% you need to define Fech (sampling frequencey) in the
workspace
    meanD2(k).dX20=mean(arrayfun(@(X)(X.dX(1).^2),trackpair(IR)));
    meanD2(k).dY20=mean(arrayfun(@(X)(X.dY(1).^2),trackpair(IR)));
    meanD2(k).dR20=binR2(k);
     clear MX2;
```

```
end


filename22 = [string_part_2 str '\meanD2_' str '\meanD2_' str '_' int2str(i) '_60ita.mat'];
filename2 =join(filename22,"");
save(filename2,'meanD2')

clearvars MX2 MY2 MR2 MD2 MRD2

Nbins=64;
%Dmax=3.828; %you have to set this value to be the maximum separation you want to explore, now it
is set for 100mm (assuming your data is in mm)
Dmax=36*ita;

dX0=arrayfun(@(X)(abs(X.dX(1))),trackpair);
dY0=arrayfun(@(X)(abs(X.dY(1))),trackpair);
dR20=arrayfun(@(X)(X.dR2(1)),trackpair);

edgesX=linspace(0,Dmax,Nbins);
edgesY=linspace(0,Dmax,Nbins);
edgesR2=linspace(0,Dmax^2,Nbins);

binX=(edgesX(2:end)+edgesX(1:end-1))/2;
binY=(edgesY(2:end)+edgesY(1:end-1))/2;
binR2=(edgesR2(2:end)+edgesR2(1:end-1))/2;

%%
[NX,binX0]=histc(dX0,edgesX);
[NY,binY0]=histc(dY0,edgesY);
[NR2,binR20]=histc(dR20,edgesR2);

for k=2:numel(binX)
 %    IX=find(binX0==k);
%     IY=find(binY0==k);
    IR=find(binR20==k);
% for statistics on 1D separation, we still condition on the 2D separation
% R20 to avoid combining for instance particles with small separation in X but actually very much
separated in Y
    IX=IR;
    IY=IR;
    dX2=arrayfun(@(X)((X.dX-X.dX(1)).^2),trackpair(IX),'UniformOutput',false);
    dY2=arrayfun(@(X)((X.dY-X.dY(1)).^2),trackpair(IY),'UniformOutput',false);
    dR2=arrayfun(@(X)(X.dR2-X.dR2(1)),trackpair(IR),'UniformOutput',false);
    dD2=arrayfun(@(X)((X.dX-X.dX(1)).^2+(X.dY-X.dY(1)).^2),trackpair(IR),'UniformOutput',false);
    dRD2=arrayfun(@(X)(X.dR2),trackpair(IR),'UniformOutput',false);

    NX=cellfun(@(X)(numel(X)),dX2);
    NY=cellfun(@(X)(numel(X)),dY2);
    NR=cellfun(@(X)(numel(X)),dR2);
    ND=cellfun(@(X)(numel(X)),dD2);
    NRD=cellfun(@(X)(numel(X)),dRD2);

    MX2=NaN(numel(dX2),max(NX));
    MY2=NaN(numel(dY2),max(NY));
    MR2=NaN(numel(dD2),max(NR));
    MD2=NaN(numel(dD2),max(ND));
    MRD2=NaN(numel(dRD2),max(NRD));

    for kk=1:numel(dX2)
        MX2(kk,1:NX(kk))=dX2{kk};
    end

    for kk=1:numel(dY2)
        MY2(kk,1:NY(kk))=dY2{kk};
    end

    for kk=1:numel(dR2)
        MR2(kk,1:NR(kk))=dR2{kk};
    end

    for kk=1:numel(dD2)
```

```
        MD2(kk,1:ND(kk))=dD2{kk};
    end

    for kk=1:numel(dRD2)
        MRD2(kk,1:NRD(kk))=dRD2{kk};
    end

    dX2=nanmean(MX2,1);
    dY2=nanmean(MY2,1);
    dR2=nanmean(MY2,1);
    dD2=nanmean(MD2,1);
    dRD2=nanmean(MRD2,1);

    dX2(dX2==NaN)=[];
    dY2(dY2==NaN)=[];
    dR2(dR2==NaN)=[];
    dD2(dD2==NaN)=[];
    dRD2(dRD2==NaN)=[];

    meanD2(k).dX2=nanmean(MX2,1);
    meanD2(k).dY2=nanmean(MY2,1);
    meanD2(k).dR2=nanmean(MR2,1);
    meanD2(k).dD2=nanmean(MD2,1);
     meanD2(k).dRD2=nanmean(MRD2,1);
    meanD2(k).TX=[0:numel(dX2)-1]/Fech;% you need to define Fech (sampling frequencey) in the
workspace
    meanD2(k).TY=[0:numel(dY2)-1]/Fech;% you need to define Fech (sampling frequencey) in the
workspace
    meanD2(k).TR=[0:numel(dR2)-1]/Fech;% you need to define Fech (sampling frequencey) in the
workspace
    meanD2(k).TD=[0:numel(dD2)-1]/Fech;% you need to define Fech (sampling frequencey) in the
workspace
    meanD2(k).dX20=mean(arrayfun(@(X)(X.dX(1).^2),trackpair(IR)));
    meanD2(k).dY20=mean(arrayfun(@(X)(X.dY(1).^2),trackpair(IR)));
    meanD2(k).dR20=binR2(k);
     clear MX2;
end



filename22 = [string_part_2 str '\meanD2_' str '\meanD2_' str '_' int2str(i) '_36ita.mat'];
filename2 =join(filename22,"");
save(filename2,'meanD2')

clearvars MX2 MY2 MR2 MD2 MRD2

Nbins=64;
%Dmax=3.828; %you have to set this value to be the maximum separation you want to explore, now it
is set for 100mm (assuming your data is in mm)
Dmax=22*ita;

dX0=arrayfun(@(X)(abs(X.dX(1))),trackpair);
dY0=arrayfun(@(X)(abs(X.dY(1))),trackpair);
dR20=arrayfun(@(X)(X.dR2(1)),trackpair);

edgesX=linspace(0,Dmax,Nbins);
edgesY=linspace(0,Dmax,Nbins);
edgesR2=linspace(0,Dmax^2,Nbins);

binX=(edgesX(2:end)+edgesX(1:end-1))/2;
binY=(edgesY(2:end)+edgesY(1:end-1))/2;
binR2=(edgesR2(2:end)+edgesR2(1:end-1))/2;

%%
[NX,binX0]=histc(dX0,edgesX);
[NY,binY0]=histc(dY0,edgesY);
[NR2,binR20]=histc(dR20,edgesR2);



for k=2:numel(binX)
```

```
 %   IX=find(binX0==k);
%    IY=find(binY0==k);
    IR=find(binR20==k);
% for statistics on 1D separation, we still condition on the 2D separation
% R20 to avoid combining for instance particles with small separation in X but actually very much
separated in Y
    IX=IR;
    IY=IR;
    dX2=arrayfun(@(X)((X.dX-X.dX(1)).^2),trackpair(IX),'UniformOutput',false);
    dY2=arrayfun(@(X)((X.dY-X.dY(1)).^2),trackpair(IY),'UniformOutput',false);
    dR2=arrayfun(@(X)(X.dR2-X.dR2(1)),trackpair(IR),'UniformOutput',false);
    dD2=arrayfun(@(X)((X.dX-X.dX(1)).^2+(X.dY-X.dY(1)).^2),trackpair(IR),'UniformOutput',false);
    dRD2=arrayfun(@(X)(X.dR2),trackpair(IR),'UniformOutput',false);

    NX=cellfun(@(X)(numel(X)),dX2);
    NY=cellfun(@(X)(numel(X)),dY2);
    NR=cellfun(@(X)(numel(X)),dR2);
    ND=cellfun(@(X)(numel(X)),dD2);
    NRD=cellfun(@(X)(numel(X)),dRD2);

    MX2=NaN(numel(dX2),max(NX));
    MY2=NaN(numel(dY2),max(NY));
    MR2=NaN(numel(dD2),max(NR));
    MD2=NaN(numel(dD2),max(ND));
    MRD2=NaN(numel(dRD2),max(NRD));

    for kk=1:numel(dX2)
        MX2(kk,1:NX(kk))=dX2{kk};
    end

    for kk=1:numel(dY2)
        MY2(kk,1:NY(kk))=dY2{kk};
    end

    for kk=1:numel(dR2)
        MR2(kk,1:NR(kk))=dR2{kk};
    end

    for kk=1:numel(dD2)
        MD2(kk,1:ND(kk))=dD2{kk};
    end

    for kk=1:numel(dRD2)
        MRD2(kk,1:NRD(kk))=dRD2{kk};
    end

    dX2=nanmean(MX2,1);
    dY2=nanmean(MY2,1);
    dR2=nanmean(MY2,1);
    dD2=nanmean(MD2,1);
    dRD2=nanmean(MRD2,1);

    dX2(dX2==NaN)=[];
    dY2(dY2==NaN)=[];
    dR2(dR2==NaN)=[];
    dD2(dD2==NaN)=[];
    dRD2(dRD2==NaN)=[];

    meanD2(k).dX2=nanmean(MX2,1);
    meanD2(k).dY2=nanmean(MY2,1);
    meanD2(k).dR2=nanmean(MR2,1);
    meanD2(k).dD2=nanmean(MD2,1);
     meanD2(k).dRD2=nanmean(MRD2,1);
    meanD2(k).TX=[0:numel(dX2)-1]/Fech;% you need to define Fech (sampling frequencey) in the
workspace
    meanD2(k).TY=[0:numel(dY2)-1]/Fech;% you need to define Fech (sampling frequencey) in the
workspace
    meanD2(k).TR=[0:numel(dR2)-1]/Fech;% you need to define Fech (sampling frequencey) in the
workspace
    meanD2(k).TD=[0:numel(dD2)-1]/Fech;% you need to define Fech (sampling frequencey) in the
workspace
```

```
    meanD2(k).dX20=mean(arrayfun(@(X)(X.dX(1).^2),trackpair(IR)));
    meanD2(k).dY20=mean(arrayfun(@(X)(X.dY(1).^2),trackpair(IR)));
    meanD2(k).dR20=binR2(k);
     clear MX2;
end


filename22 = [string_part_2 str '\meanD2_' str '\meanD2_' str '_' int2str(i) '_22ita.mat'];
filename2 =join(filename22,"");
save(filename2,'meanD2')



clearvars MX2 MY2 MR2 MD2 MRD2


Nbins=64;
%Dmax=3.828; %you have to set this value to be the maximum separation you want to explore, now it
is set for 100mm (assuming your data is in mm)
Dmax=13*ita;

dX0=arrayfun(@(X)(abs(X.dX(1))),trackpair);
dY0=arrayfun(@(X)(abs(X.dY(1))),trackpair);
dR20=arrayfun(@(X)(X.dR2(1)),trackpair);

edgesX=linspace(0,Dmax,Nbins);
edgesY=linspace(0,Dmax,Nbins);
edgesR2=linspace(0,Dmax^2,Nbins);

binX=(edgesX(2:end)+edgesX(1:end-1))/2;
binY=(edgesY(2:end)+edgesY(1:end-1))/2;
binR2=(edgesR2(2:end)+edgesR2(1:end-1))/2;

%%
[NX,binX0]=histc(dX0,edgesX);
[NY,binY0]=histc(dY0,edgesY);
[NR2,binR20]=histc(dR20,edgesR2);

for k=2:numel(binX)
 %   IX=find(binX0==k);
%    IY=find(binY0==k);
    IR=find(binR20==k);
% for statistics on 1D separation, we still condition on the 2D separation
% R20 to avoid combining for instance particles with small separation in X but actually very much
separated in Y
    IX=IR;
    IY=IR;
    dX2=arrayfun(@(X)((X.dX-X.dX(1)).^2),trackpair(IX),'UniformOutput',false);
    dY2=arrayfun(@(X)((X.dY-X.dY(1)).^2),trackpair(IY),'UniformOutput',false);
    dR2=arrayfun(@(X)(X.dR2-X.dR2(1)),trackpair(IR),'UniformOutput',false);
    dD2=arrayfun(@(X)((X.dX-X.dX(1)).^2+(X.dY-X.dY(1)).^2),trackpair(IR),'UniformOutput',false);
    dRD2=arrayfun(@(X)(X.dR2),trackpair(IR),'UniformOutput',false);

    NX=cellfun(@(X)(numel(X)),dX2);
    NY=cellfun(@(X)(numel(X)),dY2);
    NR=cellfun(@(X)(numel(X)),dR2);
    ND=cellfun(@(X)(numel(X)),dD2);
    NRD=cellfun(@(X)(numel(X)),dRD2);

    MX2=NaN(numel(dX2),max(NX));
    MY2=NaN(numel(dY2),max(NY));
    MR2=NaN(numel(dD2),max(NR));
    MD2=NaN(numel(dD2),max(ND));
    MRD2=NaN(numel(dRD2),max(NRD));

    for kk=1:numel(dX2)
        MX2(kk,1:NX(kk))=dX2{kk};
    end

    for kk=1:numel(dY2)
        MY2(kk,1:NY(kk))=dY2{kk};
```

```
    end

    for kk=1:numel(dR2)
        MR2(kk,1:NR(kk))=dR2{kk};
    end

    for kk=1:numel(dD2)
        MD2(kk,1:ND(kk))=dD2{kk};
    end

    for kk=1:numel(dRD2)
        MRD2(kk,1:NRD(kk))=dRD2{kk};
    end

    dX2=nanmean(MX2,1);
    dY2=nanmean(MY2,1);
    dR2=nanmean(MY2,1);
    dD2=nanmean(MD2,1);
    dRD2=nanmean(MRD2,1);

    dX2(dX2==NaN)=[];
    dY2(dY2==NaN)=[];
    dR2(dR2==NaN)=[];
    dD2(dD2==NaN)=[];
    dRD2(dRD2==NaN)=[];

    meanD2(k).dX2=nanmean(MX2,1);
    meanD2(k).dY2=nanmean(MY2,1);
    meanD2(k).dR2=nanmean(MR2,1);
    meanD2(k).dD2=nanmean(MD2,1);
     meanD2(k).dRD2=nanmean(MRD2,1);
    meanD2(k).TX=[0:numel(dX2)-1]/Fech;% you need to define Fech (sampling frequencey) in the
workspace
    meanD2(k).TY=[0:numel(dY2)-1]/Fech;% you need to define Fech (sampling frequencey) in the
workspace
    meanD2(k).TR=[0:numel(dR2)-1]/Fech;% you need to define Fech (sampling frequencey) in the
workspace
    meanD2(k).TD=[0:numel(dD2)-1]/Fech;% you need to define Fech (sampling frequencey) in the
workspace
    meanD2(k).dX20=mean(arrayfun(@(X)(X.dX(1).^2),trackpair(IR)));
    meanD2(k).dY20=mean(arrayfun(@(X)(X.dY(1).^2),trackpair(IR)));
    meanD2(k).dR20=binR2(k);
     clear MX2;
end


filename22 = [string_part_2 str '\meanD2_' str '\meanD2_' str '_' int2str(i) '_13ita.mat'];
filename2 =join(filename22,"");
save(filename2,'meanD2')



clearvars trackpair MX2 MY2 MR2 MD2 MRD2
end
end
```